To the Graduate Council:

I am submitting herewith a thesis written by Charles D. Stone entitled "Ferromagnetic Resonance Intensity (I_S): A Rapid Method for Determining the Mode of Origin of Lunar Glass Beads." I have examined the final copy of this thesis for form and content and recommend that it be accepted in partial fulfillment of the requirements for the degree of Master of Science, with a major in Geology.

Lawrence A. Taylor

Lawrence A. Taylor, Major Professor

We have read this thesis
and recommend its acceptance:

Otto C. Kopp

Harry G. McDonnell

Accepted for the Council:

L. Evan Pahl

Vice Chancellor
Graduate Studies and Research

3065191

FERROMAGNETIC RESONANCE INTENSITY (I_S): A RAPID METHOD FOR DETERMINING THE MODE OF ORIGIN OF LUNAR GLASS BEADS

A Thesis

Presented for the

Master of Science

Degree

The University of Tennessee, Knoxville

Charles D. Stone

December 1982

ABSTRACT

Glass beads formed by lunar fire-fountaining have been recognized in soil samples returned by the Apollo missions to the Moon. These minute droplets represent frozen samples of lunar magmas which are relatively primitive to the mare basalts. The chemistries preserved in these glass particles are essential to any petrogenetic considerations of the early Moon.

Glass beads originating from impact processes (i.e., shock melting by meteorites) are abundant throughout the Apollo soil collections. The chemistries recorded by the impact beads can represent melts of a regolith (composed of grains and fragments of rock, mineral, and meteorite, and also previous impact melts), or the chemistry may reflect the melt from a rock unit or a combination of units.

Cursory inspection of volcanic and impact beads usually will not allow their discrimination on the basis of origin. The difficulty of discerning a bead's mode of origin has led to the test of a new criterion: the intensity of ferromagnetic resonance (I_s) of a bead. This technique can be employed for rapid screening to determine the origin of the glass beads.

The ferromagnetic resonance method relies on the detection of magnetically single-domain Fe formed during impact melting by auto-reduction of Fe^{2+} in the melt. In order to establish the usefulness of I_s, extensive scanning electron microscope (SEM) inspection of glass bead surfaces was conducted which provided reliable evidence of the mode of glass genesis. I_s was tested against the

"type" Apollo 15 and Apollo 17 volcanic glass beads. Additional volcanics were also found during the course of the study. Of the volcanic glasses, 94% have I_s values less than one, implying the absence of single-domain Fe. Moderate to high I_s values (10 to 270) were recorded in 75% of the impact beads. The remaining impact beads have I_s values less than one. These samples lack single-domain Fe and could represent impact melts of bedrock with little or no contribution from the regolith. The ability to discriminate bedrock-derived impact melts as opposed to impact melts partially or completely from the regolith is an additional important potential for the ferromagnetic resonance technique.

PREFACE

A large portion of the work in this study is represented by scanning electron microscopy. Many of the resulting photomicrographs have been incorporated in the appendices in order to illustrate various surface features of the glass beads. Many of these features are referred to directly in the text. However, to avoid confusion for the reader, to allow a fuller vista of the features, and to preserve the continuity of the individual appendices, all photomicrographs have been confined to the appendices.

TABLE OF CONTENTS

CHAPTER		PAGE
I.	INTRODUCTION AND PREVIOUS WORK	1
II.	THEORETICAL BASIS FOR THE USE OF FERROMAGNETIC RESONANCE INTENSITY AS A CRITERION FOR THE DETERMINATION OF GLASS BEAD ORIGIN	6
	Formation of Auto-reduced Fe	6
	Detection of Auto-reduced Fe	9
	Use of FMR as an Exposure Age Indicator for Soils	10
	Use of FMR as an Indicator of Glass Bead Origin	10
III.	DETERMINING ORIGIN OF GLASS BEADS BY SCANNING ELECTRON MICROSCOPY	12
	Characteristics of Volcanic Glass Beads	12
	Characteristics of Impact Glass Beads	15
IV.	EXPERIMENTAL PROCEDURE	18
V.	FMR AND CHEMICAL DATA FOR VOLCANIC AND IMPACT GLASS BEADS	20
	Volcanic Glasses	20
	Impact Glasses	23
	Comparison of Volcanic and Impact Glass Data	23
	Discussion	29
VI.	CONCLUSION	39
LIST OF REFERENCES		42
APPENDICES		50

CHAPTER PAGE

APPENDIX A. AGGLUTINATE PARTICLES 51

APPENDIX B. VOLATILE-RICH MICROMOUND COATINGS ON VOLCANIC BEADS 54

APPENDIX C. Fe-RICH PLATELETS ON VOLCANIC BEADS 58

APPENDIX D. VOLCANIC COMPOSITE MORPHOLOGY 60

APPENDIX E. OUTGASSING PORES ON IMPACT BEADS 64

APPENDIX F. AUTO-REDUCED NATIVE Fe MICROMOUNDS ON IMPACT BEADS 67

APPENDIX G. FORMATIONS OF AMEOBOID/"LACY" IRON ON IMPACT BEADS 72

APPENDIX H. IRON MICROMOUNDS WITH VOLATILE "WAISTS" ON IMPACT BEADS 75

APPENDIX I. SECONDARY IMPACTS ON GLASS BEADS 77

APPENDIX J. SURFACE ACCRETIA 82

APPENDIX K. MISCELLANEOUS FEATURES 86

VITA 89

LIST OF TABLES

TABLE		PAGE
I.	Description of Volcanic Glasses	21
II.	Description of Impact Glasses	25
III.	Volcanic Glass Compositions	30
IV.	Impact Glass Compositions	35
V.	Impact Glass Chemical Compositions Compared to Previously Reported Bedrock-Derived Glass Compositions	38

LIST OF FIGURES

FIGURE		PAGE
1.	Fe Metal Inclusion Types and Sizes in Lunar Glasses and the Stability Size Range for Single Domain Particles	8
2.	FMR Data for Volcanic Spherules	22
3.	FMR Data for Impact Beads	24
4.	A Compilation of the Various Diagnostic Features Used to Determine Glass Bead Origin and Their Corresponding FMR Data	27
5.	FMR Data for Volcanic and Impact Droplets Shown in Direct Comparison	28
6.	Plot of Volcanic and Impact Beads with $I_s < 1$	31
7.	FeO vs I_s for All Impact Beads in This Study	33

CHAPTER I

INTRODUCTION AND PREVIOUS WORK

A wide variety of particles populate the soil samples which were returned from the Moon by the Apollo and Luna missions, including meteoritic fragments, mineral and lithic fragments, agglutinates and microbreccias, and glass particles of various affinities. The glass particles, ubiquitous in the <1mm soil fractions, are potentially very significant for lunar petrogenesis. They occur in a wide assortment of colors and local abundances (Heiken, 1974; 1975; Heiken and McKay, 1974; Basu and Bower, 1977).

As quench samples of a melt, glass beads record and preserve the chemistry of a liquid. However, for this chemistry to be meaningful, the origin of the melt must be known. Puzzlement over the origin of these beads has led to the postulation of four possible models of glass bead formation (e.g., Prinz et al., 1973; Roedder and Weiblen, 1973): a) meteoritic impact on solid lunar crust (i.e., impact melting); b) direct condensation from a vapor; c) meteoritic impact on lava lakes with glass forming from the subsequent splash; and d) glass produced from volcanic fire-fountaining. Most workers consider that the first and last (i.e., a and d) origins are prevalent.

Those spherules produced during impact melting are the most abundant type in the lunar soils. The information contained within this glass type can give important insight into the nature of the source material. Several studies have shown that glasses of impact origin can be related to known rock types (e.g., Keil et al., 1971; Reid et al., 1972a; 1972b; Ridley et al., 1973; Norman et al., 1977; 1978).

The volcanic glass beads formed during lunar lava-fountaining on the other hand, may contain considerable information on endogenetic lunar processes. The volcanic vents which produce these glasses are considered to be direct conduits from shallow magma chambers (Adams et al., 1974; Housley, 1978). Hence, the chemical compositions of these particles may be related to primary magmas and their fractionation products.

The importance of the volcanic glasses requires that a reliable, rapid, and non-destructive method be established to discriminate between volcanic glass beads and glass spherules produced by impact processes. Determination of glass bead origin has been based on various criteria, each of which are ambiguous. Collectively, these criteria are good indicators of origin; however, over-dependence on one or a few of these features can lead to misinterpretation of origin. These various criteria include:

Shape of Bead. Roedder and Weiblen (1973) suggested that shapes formed in response to high shear-stress rates (i.e., oblate spheroids) do not occur in volcanic beads. However, in contradiction to this assertion, oblate spheroids, prolate spheroids, teardrops, and irregular shapes, as well as spheres, do occur in beads interpreted to be volcanic (McKay and Heiken, 1973; McKay et al., 1973; Haggerty, 1974).

Inclusions. The inclusion of mineral grains within glass beads has been used to imply impact-melt origin (Simonds et al., 1977; Fruland et al., 1977). Such inclusions indicate that only a partial

digestion and incorporation of target material has occurred in the formation of the glass during impact. However, most glass spheres, judged to be of impact origin on the basis of other criteria, lack inclusions. Euhedral crystals, olivine in particular, occurring in glass beads have been used to indicate a volcanic origin for the glasses (Reid et al., 1972b; McKay and Heiken, 1973; Prinz et al, 1973). These crystals probably represent crystallization of liquid prior to and during lava-fountaining. This is considered evidence for fractionation and indicates a non-primary nature for the melt, as seen in the glass. However, it may not always be possible to determine whether a given mineral inclusion is an impact-derived fragment or a true phenocryst. Furthermore, euhedral crystals have formed in some ropy glasses interpreted as impact-produced (Fruland et al., 1977).

Chemical Homogeneity. The lunar soils provide a diverse assemblage of particles which combine to produce a heterogeneous target material for impact melts. The resulting glasses can also reflect that heterogeneity within a single bead (Warner et al., 1979). However, superheating of the melt due to an intense impact may allow for complete assimilation and homogenization of target material in the melt. As a result, some impact glasses can be homogenous (e.g., Reid et al., 1972b; Warner et al., 1979). However, all beads interpreted to be volcanic appear to be internally homogenous (e.g., Reid et al., 1972b).

Schleiren. This feature records the incomplete assimilation of target material and is not characteristic of volcanic glasses.

Although indicative of impact melting, schleiren are not common and can only be observed in thin section (McKay et al., 1973; Cavarretta et al., 1972).

Bubbles. Vaporization of volatile elements evolved during impact melting creates bubbles in the melt (Carter, 1973). These can be frozen into the glass. Volcanic glass beads also have been observed to contain similar bubbles interpreted as due to trapping of volatile material during fire-fountaining. Indeed, bubbles are common in the orange glass beads of volcanic origin in 74001 (McKay and Heiken, 1973).

Compositional Groupings. Restricted compositional clusters for a number of beads are interpreted as suggestive of volcanic origin (Delano, 1981). However, impact glasses also form compositional clusters (e.g., Reid et al., 1972a; 1972b). Additionally, this method requires many glass particles and a statistical treatment; obviously this is not a practical criterion for use on single spherules.

Ni Abundances. Glass beads of impact origin may contain siderophile elements (e.g., Ni) derived from the impacting meteorite. Delano et al., (1981) contend the distribution of this contamination should be non-uniform, and that the resulting heterogeneity will be reflected by different Ni abundances within a single glass particle. However, as with chemical homogeneity discussed above, superheating can completely homogenize a silicate melt. In addition, this criterion requires extensive careful electron microanalyses and cannot provide

for a rapid screening of individual spherules.

Surface Features. Various surface features visible with a scanning electron microscope (SEM) are apparently unique and if present, can accurately characterize a glass bead's origin. Characteristic micromound deposits of volatile material coating primary surfaces appear to be confined to beads of volcanic fire-fountain origin (e.g. McKay et al., 1973; Butler and Meyer, 1976). Composite forms are common in volcanic beads but are rare in impact droplets. Other surface features such as native Fe micromounds are apparently found only on beads of impact origin (e.g. Carter and McKay, 1972). A variety of SEM features were used to first support the hypothesis that Apollo 15 green glass beads were volcanic (McKay et al., 1973). Though SEM may be a reliable method in the determination of glass bead genesis, it involves a tedious, time-consuming technique.

Of the various criteria discussed above for glass bead origin, the SEM-observed features are probably the best. The other criteria have a more limited applicability. However, all of the above criteria involve destructive techniques and are time-consuming. These considerations have been paramount in the search for a criterion for the recognition of glass bead genesis which involves the rapid, non-destructive screening of individual particles.

CHAPTER II

THEORETICAL BASIS FOR THE USE OF FERROMAGNETIC RESONANCE INTENSITY AS A CRITERION FOR THE DETERMINATION OF GLASS BEAD ORIGIN

The use of ferromagnetic resonance (FMR) intensity (I_s) is proposed as a criterion which can determine the origin of a glass bead. FMR spectroscopy is capable of detecting the presence of auto-reduced single domain Fe with very high sensitivity (Stone and Taylor, 1982a; 1982b). It is this species of Fe metal, unique to regolith processes which contributes exclusively to FMR intensity.

Formation of Auto-Reduced Fe

Early studies on agglutinate particles showed them to be lithic, mineral, meteorite, and glass fragments bonded together by a glass matrix (Agrell et al., 1970; Duke et al., 1970). Examples of agglutinate particles are presented in Appendix A. The agglutinates are produced by micrometeorite impacts which form the glass matrices by shock melting the target regolith. Their abundance in a soil is related to the exposure age of that soil (McKay et al., 1972).

Several workers (e.g., Agrell et al, 1970; Housley et al., 1970; 1972; 1973; and Mehta and Goldstein, 1979) reported the presence of "fine-grained" Fe-metal particles disseminated throughout agglutinitic and breccia glasses. Direct measurements of the native metal by transmission and scanning electron microscope images showed them to range in size from as small as 20Å to greater than 330Å. This Fe-metal type is markedly different in its chemistry and genesis from other

metallic inclusions also found in lunar glasses. Many investigators (e.g., Goldstein et al. 1970; 1973; 1974; Mehta and Goldstein, 1979) have described Fe-Ni-Co metallic alloys compounded with varying amounts of P, S, and C. These grains are much larger than 330Å and many are probably of meteoritic origin. Morris (1980) showed that Fe-metal particles generated from igneous rocks and breccias by comminution processes are also larger than 330Å. The auto-reduced Fe, in contrast, is entirely Fe (Mehta and Goldstein, 1979).

Figure 1 illustrates the relative grain sizes for the metallic inclusions found in the lunar glasses. In volcanic glasses native Fe metal, if present, exists to an upper size limit approximately that of the unit cell size for Fe metal. The lower size limit for auto-reduced Fe has been observed at approximately 20-40 Å (Housley et al., 1973) but probably extends to a few Å. The upper limit has been observed to several thousands of angstroms. Finally, the range of sizes for metallic particles derived from comminution of rocks and from meteorites is shown. The lower size limit of these particles may extend to approximately 350 Å but is usually much larger.

Housley et al. (1973; 1974) describe an auto-reduction process which accounts for the formation of the fine-grained, native-Fe metal. Specifically, soil particles at the surface of the lunar regolith are exposed to solar-wind elements (particularly H and C). These elements are implanted into the surface of soil grains incident to the solar wind. During micrometeorite-induced shock melting of the regolith the trapped elements are released as gases which impose a highly reducing environment (low fO_2) causing reduction of Fe^{2+} in the melt to native

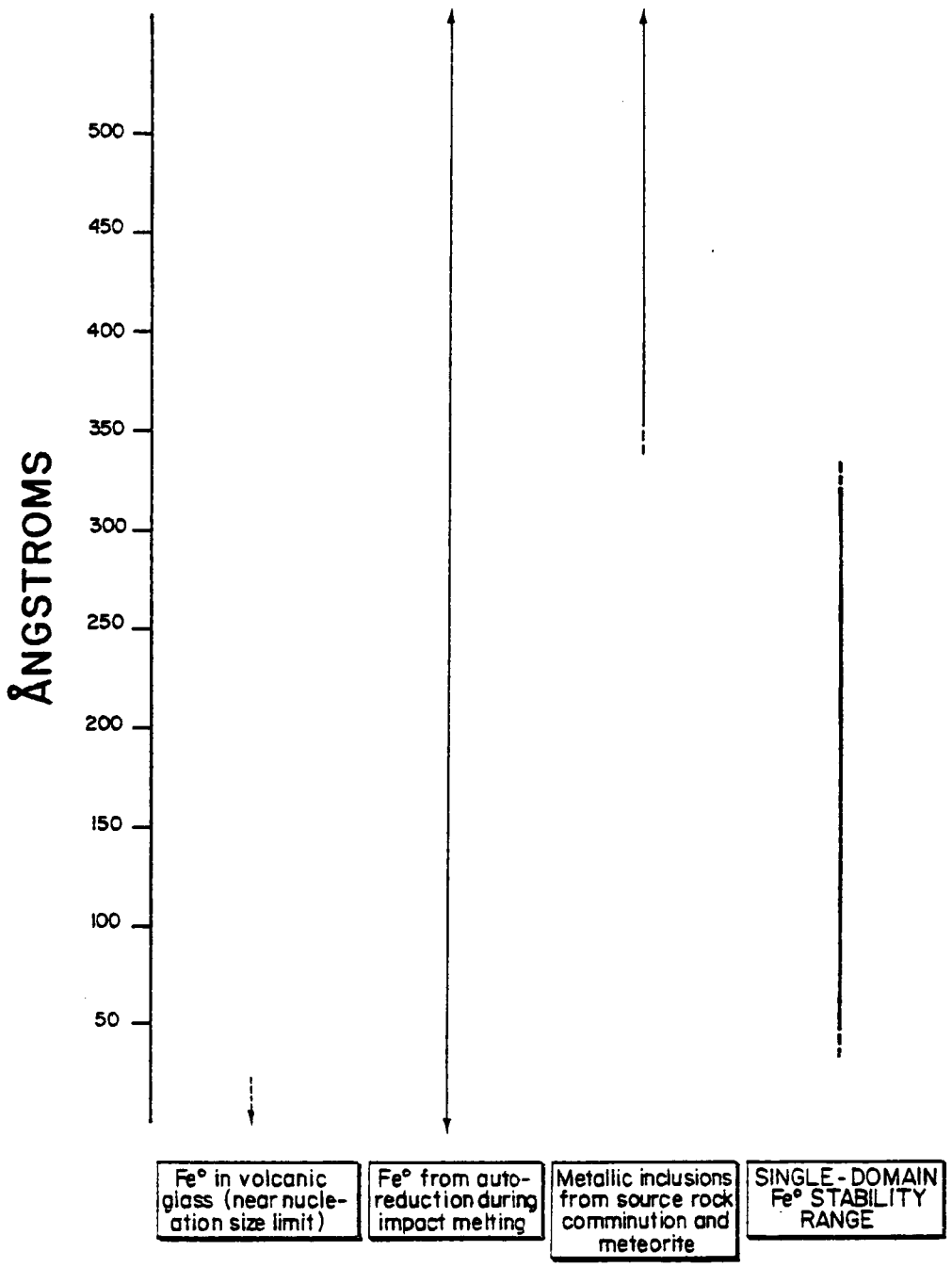


FIGURE 1. Fe metal inclusion types and sizes in lunar glasses and the stability size range for single-domain particles.

Fe. It is the resulting Fe from auto-reduction which is the fine-grained metal phase found so widely disseminated throughout agglutinitic glass and breccias.

Detection of Auto-reduced Fe

The presence of auto-reduced, fine-grained native Fe can be detected through the use of electron paramagnetic resonance (EPR) spectroscopy. This is accomplished by subjecting a sample to a varying magnetic field strength and measuring the absorbed microwave energy associated with changes in electron-spin directions. For Fe metal, "characteristic" ferromagnetic absorption spectra can be produced only in the presence of single-domain Fe. Single-domain particles are ones which are uniformly magnetized. Figure 1 also shows the size range for the stability of the single-domain configuration for Fe grains. The size requirement for such magnetically ordered units is well defined. The individual grains must be between 40Å and 330Å Housley, 1976). Significantly, the size range for single-domain stability only coincides with the size range of native Fe° grains produced by auto-reduction. Hence, the existence of single-domain Fe° implies a single process is responsible for its formation, meteoritic impacts of the regolith.

A measure of the relative quantity of single-domain Fe can be accomplished by calculating the intensity of ferromagnetic resonance (I_s). I_s is a dimensionless parameter derived from the amplitude and width of the "characteristic" absorption spectrum induced by single-domain particles as measured by an electron paramagnetic spectrometer (EPR).

Use of FMR as an Exposure Age Indicator for Soils

Ferromagnetic resonance intensity (I_s) varies with the quantity of impact auto-reduced Fe contained within a soil. When I_s is normalized to total FeO content (determined either chemically or magnetically) of the soil (i.e., I_s/FeO), the value represents a relative index for soil maturity (Morris, 1976). The higher the I_s/FeO value, the longer a soil has been subjected to processes at the lunar surface (i.e., solar wind implantation and micrometeorite impact).

That I_s/FeO can serve as a realistic indication of exposure times has been demonstrated by several studies. Implanted N, C, and Ar gases which originate from solar wind (Chang et al., 1973; Muller, 1974; Eberhardt et al, 1972) were shown by Morris (1976) to increase to concentration with increasing I_s/FeO values. Agglutinitic particles also provide evidence for the validity of I_s/FeO as a maturity index. The concentrations of these micrometeorite-produced grains increase with soil maturity (McKay et al., 1974). Morris (1976) also showed that I_s/FeO values increase with higher concentrations of agglutinate. All indications point to FMR as a dependable measure of soil maturity. Indeed, such measurements are routinely made on lunar core samples (e.g., Morris, 1978a; 1978b; 1978c; Morris and Gose, 1978; Morris et al., 1978) to produce exposure age profiles.

Use of FMR as an Indicator of Glass Bead Origin

As an extension of the use of I_s, this study sought to apply its

use to individual glass beads from lunar soils in order to gain insight into their origin. Glass beads produced from meteorite impact melting of the regolith should contain single-domain Fe. The unique signature of this metal can then be measured. High values of I_s are consistent with an impact origin. Beads with relatively low or no I_s could be volcanic in origin. In order to adequately correlate the type of grain (volcanic versus impact) to I_s data, extensive use was made of the SEM.

CHAPTER III

DETERMINING ORIGIN OF GLASS BEADS BY SCANNING ELECTRON MICROSCOPY

As a test of the FMR criterion, a correlation of beads of known affinities with I_s values was required. In order to establish a bead's origin with certainty, a set of surface features visible only with the aid of a scanning electron microscope (SEM) was employed. Surface characteristics of glass beads possess unique, definitive information pertinent to their origin. These diagnostic features are discussed below in detail, and scanning electron photomicrographs are included in the Appendices.

Characteristics of "Type" Volcanic Glass Beads

Historically, the recognition of volcanic glass beads was based on a wide variety of SEM, morphologic, textural, and chemical criteria. The descriptions of these features come from two sample suites: Apollo 15 green- and Apollo 17 orange- and black-glass beads.

Thin coatings of volatile-rich micromounds were discovered during inspection by SEM on the surfaces of Apollo 15 green and Apollo 17 orange glasses (McKay et al., 1973; Clanton et al., 1978). Compositional analyses of these coatings showed they are composed of S, Zn, K, Cl, Ni, and P in varying amounts (Meyer et al., 1975; Butler and Meyer, 1976). Butler and Meyer (1976) suggested that the varying thickness of the coatings, together with their relatively constant compositions indicate the coats accumulated on bead surfaces

immediately following solidification of glass in free space . Scrapes in the coatings described by McKay et al. (1973) and Clanton et al. (1978) appear to be the result of mutual collisions of glass beads while in flight. (See Appendix B).

Surface coatings of Apollo 15 green and Apollo 17 orange spheres are enriched in volatile elements compared to the interiors of the glasses. Chou et al. (1975) and Wasson et al. (1976) explained that the sublimate was the result of condensation from a magmatic gas phase which was the propellant responsible for the expulsion of the melt during lava-fountaining. The high volatile/glass ratio seems to rule out possible formation due to splash from a lava lake caused by a meteorite impact. Significantly, similar coatings have been described on terrestrial volcanic glass beads originating from lava fountains at Mauna Ulu, Hawaii (McKay et al., 1973; Ladle, 1978).

Minute, equant, subangular crystals about 0.5 μm in long dimension are found on primary surfaces of both Apollo 15 green (McKay et al., 1973) and Apollo 17 orange glasses (Bell et al., 1974). Bell et al al. (1974) found these features to be 80%-90% Fe with Cu, Ti, and Cl accounting for the remainder of the composition. McKay et al. (1973) suggested that these Fe-rich platelets were formed by a reduction process during the early stages of formation of the glass beads. Supportive evidence for their timing includes the facts they are found only on primary surfaces of droplets and the occurrence of volatile-rich micromounds found overlying many of the platelets. (See Appendix C).

Black-glass droplets from 74001/74002 and 74220 and the cloudy

green-glass beads in 15401, 15425, 15426 and 15427 exhibit a unique composite morphology. These glass grains are generally elongate but are covered with mounds and protuberances which display various degrees of wetting with the substrate (Agrell et al., 1973; Carter et al., 1973; Clanton et al., 1973; McKay and Heiken, 1973; McKay et al., 1973), as seen in Appendix D. The rounded mounds covering these beads are the same composition as the substrate. The surfaces of these beads contain volatile coats similar to those which cover the orange- and green-glass spherules. This morphology is considered to be due to aggregations of molten globules during fountaining. Devitrification is common in the composite beads. Agrell et al. (1973) and Haggerty (1974) found the products of devitrification to be feathery ilmenite and barred olivine crystals. These are visible commonly at the surface of the composite beads (Appendix D). In fact, Haggerty (1974) showed the dark color of the composite Apollo 17 glasses to be directly related to the degree of devitrification and that the devitrification process began at the surface and proceeded inward.

^{40}Ar-^{39}Ar dating of the green and orange glasses reveals further associations with volcanism. The Apollo 15 green glass has an age of about 3.3 AE (Huneke et al., 1974) which is close to the ages of Apollo 15 mare basalts determined from Rb-Sr dating (Papanastassiou and Wasserburg, 1973). Apollo 17 orange glasses yield an ^{40}Ar-^{39} Ar age of about 3.7 AE (Schaeffer and Husain, 1973). This age links them to Apollo 17 basalt Rb-Sr dates (Tera et al., 1974).

Dark-mantle deposits also connect the green and orange glasses to a pyroclastic origin. These deposits are low-albedo features which

vary in areal extent on the moon's surface. The orange glass at Apollo 17 was sampled directly from such a dark-mantle region (Lucchita and Schmitt, 1974). Other such regions are scattered about the edges of many mare (Pieters et al., 1973; Adams et al., 1974; Head, 1974; Wolfe et al., 1975). Spectral reflectance studies of these areas indicate they consist of similar type deposits to the Apollo 17 pyroclastics (Pieters et al., 1973; Adams et al., 1974). The restriction of these deposits to mare edges is due to the deep-seated faulting which is expressed as curvilinear rilles concentric to mare basins. Stresses due to loading of basalts onto the crust during flooding may activate these faults providing conduits for lava fountaining and result in pyroclastic deposits (Solomon and Head, 1979).

The large body of evidence supporting the pyroclastic origin of the Apollo 15 green glass and the Apollo 17 orange and black glass allows them to be considered as valid "type" volcanic glasses. The test of the FMR criterion on the "type" volcanics was accomplished by assigning individual beads to the "volcanic" category on the basis of SEM observations of composite morphology, volatile-rich micromound coatings, and Fe-rich platelets and then compiling compositional data on these features by using Energy Dispersive X-ray (EDX) techniques.

Characteristics of Impact Glass Beads

All glass beads lacking the unique characteristics related to the volcanic beads, as established by the "type" volcanic beads, are categorized as impact-produced. The impact glass beads are also recognizable by their own set of distinctive morphologic features.

These features include the following:

Outgassing Pores. These structures are the surface expression of internally generated volatiles which escaped the glass during impact-produced melting (Carter, 1971; 1973; Carter and McKay, 1972). They are similar to outgassing pores found on agglutinates and are often smaller and more abundant than pores found on "type" volcanic beads. (See Appendix E).

Iron Micromounds. These small (<250Å - > 1000Å) surface features composed of native Fe are probably the direct results of the auto-reduction by H and C during impact melting. The relatively large size of the Fe micromounds in Appendix F is explained by the heterogenous nucleation of Fe. On the surface of a bead, Fe micromounds are established at rapidly-formed nucleation sites which continue to grow rapidly. Inside the bead, nucleation is more disseminated, and growth of individual grains is considerably slower resulting in smaller grains.

Amoeboid/"Lacy" Iron. This relatively rare form of native Fe, which has a dendritic, sometimes delicate form (Appendix G), is considered to be due to rapid condensation and precipitation from a vapor probably produced during impacts (Carter, 1971; 1973; Carter and McKay, 1972).

Iron Micromounds with Volatile "Waists". These Fe metal features occur less frequently than Fe micromounds but are of the same origin as other Fe micromounds. They are distinguished by the volatile-rich

coating predominated by S and P which may coat either the entire mound or, more commonly, forms a rim at the bead/mound interface (Carter, 1971; 1973; Carter and McKay, 1972). (See Appendix H.).

None of the above features have been reported on "type" volcanic beads and are unique to the impact droplets. The lack of volcanic features (volatile-rich coatings, composite morphology, and Fe-rich platelets) plus the presence of impact-related features, as described above, were used to classify glass beads as impact-produced.

CHAPTER IV

EXPERIMENTAL PROCEDURE

Individual glass beads and fragments were handpicked from each Apollo mission. Beads selected were classified initially as to color (black, brown, purple, red, orange, yellow, green, and colorless). They ranged in diameter from about 50 μm to over 500 μm; the masses of the glass beads ranged from less than 0.5 μg to more than 300 μg. Each bead was placed in a suprasil tube and measured at room temperature using a Varian E-12 Electron Paramagnetic Resonance (EPR) spectrometer. Certain elements (e.g., Fe) have unpaired electrons. An external magnetic field induces a flip in the electron spin direction. The EPR spectrometer produces a polarizing magnetic field which causes a spin-direction flip in electrons with a low-energy spin to that of a high-energy spin configuration. This change in spin direction is accompanied with an absorption of a characteristic energy, as dictated by quantum mechanics. This characteristic energy is in the microwave range (9.54 GHz). The EPR spectrometer provides a microwave source which can be "tuned" to the precise microwave frequency. The spectrometer only can measure the microwave absorption for single domain particles, and the amount of absorption can be measured as the intensity of ferromagnetic resonance and reflects the relative amount of single-domain Fe metal. Each spectrum was scanned over a magnetic field range of 0 to 10,000 Gauss in eight minutes. In order to quantitatively determine the intensity, a second spectrum was taken over a narrower range (2,000 Gauss). The resulting spectra are first

derivatives of the absorption. The values of I_s are relative to the same standard as used by Morris (1976; 1978; 1980). In addition, backgrounds were taken before and after each set of runs and compared for drift.

After FMR data were obtained, the glass beads were analyzed with a JEOL JSM U-3 scanning electron microscope equipped with a Princeton Gamma Tech 1000 energy-dispersive X-ray analysis system which allowed semi-quantitative chemistry to be performed on the various surface features. The SEM was operated at either 7 or 25 keV. All grains were coated with Au-Pd.

The final step in the procedure consisted of analysis of chemical composition of the glass beads with a MAC automated 400S electron microprobe. Each bead was mounted in epoxy and prepared as a polished section to a flat surface before analysis. Microanalyses were performed at 15 keV and a beam current of 40 nanoamps with a slightly defocused beam of about 7-10 μm diameter. Matrix corrections were applied according to the procedure of Bence and Albee (1968) using data from Albee and Ray (1970).

CHAPTER V

FMR AND CHEMICAL DATA FOR VOLCANIC AND IMPACT GLASS BEADS

The results of the test for I_s as a valid criterion for the discrimination of glass bead origin are summarized in this section. I_s values and chemical compositions for all glass droplets examined in this study are presented below. Interpretation of these results is also discussed.

Volcanic Glasses

Table I lists characteristic features and I_s values for the 34 volcanic glass spherules which survived all phases of the study. Figure 2 presents the FMR data for the "type" volcanics from 15401, 74002, and 74220. As expected, all but one of these samples have an I_s value which is essentially equal to zero. The "anomalous" bead contains a zap pit, indicating reworking (Appendix B), suggesting the moderate value of I_s may be due to the small amount of impact glass formed by the micrometeorite zapping.

During the course of this study, beads from missions other than those which contain "type" volcanics were found to possess scraped volatile-rich coats similar to the green and orange glasses (Appendix B). These are considered to be volcanic as well and, correspondingly, are also included in Figure 2. Their low I_s values are also in accordance with a volcanic origin. One notable exception is a droplet from sample 14148. This bead also shows evidence for significant

TABLE I

Description of Volcanic Glasses

Sample Number	Color	weight (μg)	I_s	Comment
10084,853 - 95	Red	4.5	0.00	M
10084,853 - 142	Red	5.2	0.00	M
14148,23 - 39	Green	5.2	10.01	M
14148,23 - 40	Green	16.4	0.00	M
15401,14 - 13	Green	222.2	0.00	M
15401,14 - 14	Green	123.9	0.00	M
15401,14 - 16	Green	64.1	0.00	C,M
15401,14 - 68	Green	103.4	0.00	M
15401,14 - 73	Green	86.1	0.28	M
15401,14 - 74	Green	62.4	0.00	M
15401,14 - 145	Green	26.0	0.20	M
15401,14 - 146	Green	18.1	19.17	M
15401,14 - 147	Green	48.0	0.00	M
15401,14 - 148	Green	70.5	0.00	M
74002,176 - 127	Orange	4.8	0.00	M
74002,176 - 129	Orange	5.1	0.00	M
74220,2 - 11	Black	338.3	0.26	C,M
74220,6 - 18	Black	115.0	0.37	C,M
74220,6 - 19	Orange	35.0	0.00	C,M
74220,6 - 97	Orange	38.9	0.00	M
74220,6 - 98	Orange	23.6	0.00	M
74220,6 - 99	Orange	26.6	0.00	M
74220,6 - 100	Orange	23.0	0.00	M
74220,6 - 101	Orange	16.0	0.00	M
74220,6 - 102	Orange	20.4	0.00	M
74220,6 - 104	Orange	18.4	0.00	M
74220,6 - 105	Orange	23.0	0.00	M
74220,6 - 106	Orange	22.9	0.00	M
74220,6 - 107	Orange	14.2	0.00	M
74220,6 - 108	Orange	23.0	0.00	M
74220,6 - 109	Orange	21.0	0.00	M
74220,6 - 110	Orange	14.1	0.00	M
74220,6 - 111	Orange	17.4	0.00	M
74220,6 - 112	Orange	18.3	0.00	M

C = Composite morphology
M = Micromound volatile-rich coating

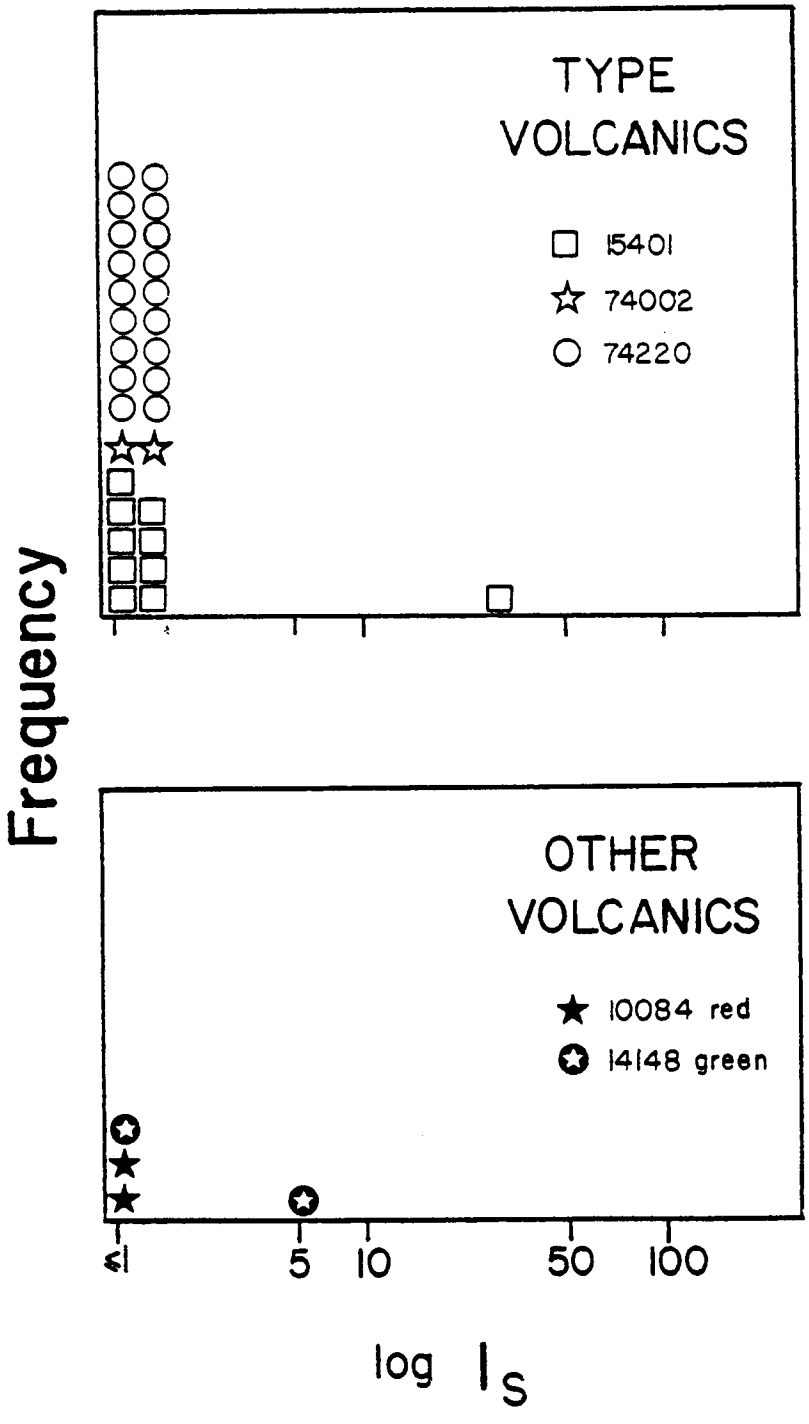


FIGURE 2. FMR data for volcanic spherules.

reworking whereby it may have acquired a minor amount of impact glass. (See Appendix B-5 and B-6).

Impact Glasses

The distribution of the 67 impact glass droplets vis-a-vis their I_s values is shown in Figure 3. Table II summarizes the descriptive information for the impact beads. Of the impact beads in this study, 75% have values of $I_s > 1$. These results are in keeping with the FMR model and denote the presence of single-domain Fe.

Comparison of Volcanic and Impact Glass Data

The direct comparison of FMR data of the volcanic and impact beads suggests the validity of the technique as an indicator of origin. A compilation of some of the most diagnostic surface features and the corresponding I_s data is summarized in Figure 4. Those beads with features which are attributed to volcanic processes are predominantly in the lowest range of I_s values. Glass beads which have diagnostic features related to impact processes have I_s values in a much higher range. Features characteristic of either impact or volcanic beads were never found together on a bead.

The distribution of I_s for all volcanic and impact beads is summarized in Figure 5. As can be seen, there are two well-defined populations in the distribution. This bimodal nature is comprised of the low I_s volcanic glasses (94% with $I_s < 1$) and the high I_s impact glasses (75% with $I_s > 1$). The evaluation of these data and discussion above support the application of FMR as a rapid screening method.

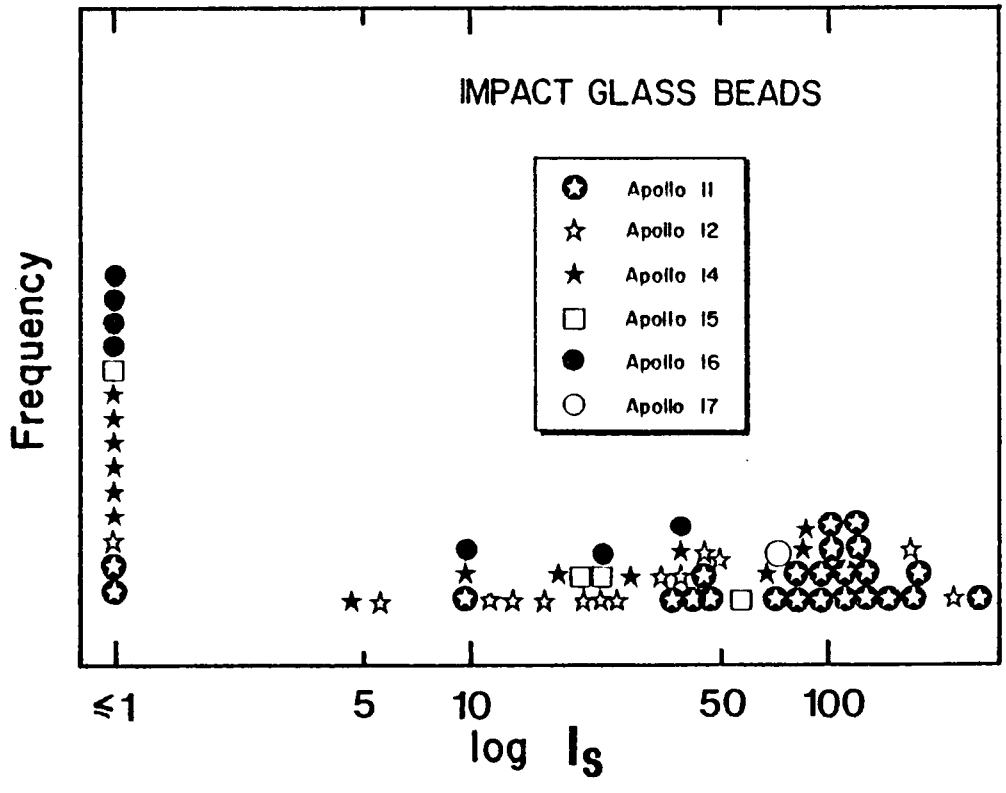


FIGURE 3. FMR data for impact beads.

TABLE II

Description of Impact Glasses

Sample Number	Color	Weight (μg)	I_s	Comment
10011,11 - 76	Black	52.0	49.00	V, Fe
10084,853 - 4	Red	379.6	74.80	Fe
10084,853 - 5	Red	87.6	13.80	
10084,853 - 6	Brown	256.6	44.50	V
10084,853 - 7	Purple	14.8	89.00	V, Fe
10084,853 - 8	Black	25.4	84.60	V, Fe, L
10084,853 - 77	Black	51.2	93.50	V, Fe
10084,853 - 78	Black	5.0	216.10	V
10084,853 - 79	Black	12.9	132.30	V, Fe, L
10084,853 - 80	Black	15.6	93.50	V, Fe
10084,853 - 82	Orange	13.6	178.20	Fe
10084,853 - 84	Orange	20.0	83.31	V, Fe, W
10084,853 - 86	Brown	36.4	161.70	V, Fe
10084,853 - 90	Red	6.4	110.57	Fe
10084,853 - 94	Red	3.4	0.00	
10084,853 - 95	Red	4.5	0.00	V
10084,853 - 137	Orange	7.3	116.00	V
10084,853 - 138	Orange	5.2	108.50	
10084,853 - 140	Orange	1.3	0.00	
10084,853 - 143	Red	5.0	101.90	
10084,853 - 149	Red	10.9	110.10	V, Fe, W
10084,853 - 150	Black	10.5	38.01	V, Fe, W
10084,853 - 151	Black	10.5	97.65	
10084,853 - 152	Red	6.5	44.26	
10084,853 - 153	Red	7.0	90.73	V
12001,7 - 3	Brown	279.8	7.07	V, Fe
12001,7 - 23	Orange	74.9	37.07	
12001,7 - 47	Black	44.3	46.83	V
12001,7 - 48	Red	15.6	46.83	V
12070,29 - 50	Black	26.0	38.09	V, Fe, L
12070,29 - 51	Black	48.5	176.30	V, Fe
12070,104 - 1	Black	63.8	20.00	
12070,104 - 49	Red	5.2	0.00	
12070,104 - 53	Yellow	3.5	12.84	
12070,104 - 55	Colorless	21.0	12.31	
12070,104 - 154	Black	9.2	30.12	V, Fe
12070,104 - 156	Black	10.9	49.04	V, Fe, L, W
12070,104 - 157	Red	5.4	23.90	
12070,142 - 52	Yellow	2.5	254.50	
14003,28 - 63	Colorless	11.1	28.30	V
14141,30 - 36	Yellow	1583.0	6.53	
14141,30 - 44	Yellow/ Green	44.0	0.00	
14141,30 - 165	Red	3.6	0.00	
14148,23 - 34	Black	40.0	41.37	V, Fe, W
14148,23 - 35	Black	15.0	81.30	V

TABLE II (continued)

Sample Number	Color	Weight (μg)	I_s	Comment
14148,23 - 37	Yellow	10.0	0.00	V
14148,23 - 41	Purple	6.0	0.00	V, Fe
14148,23 - 163	Red	5.7	84.24	
14149,39 - 164	Black	27.0	72.41	V, Fe
14156,23 - 59	Colorless	20.4	0.43	V
14156,23 - 62	Orange	10.9	14.44	
14156,23 - 167	Yellow	5.8	0.00	
14156,23 - 168	Red	14.2	23.07	V, Fe
15401,14 - 57	Orange	20.3	58.24	
15401,14 - 58	Orange	10.5	0.00	V
15401,14 - 64	Black	13.2	17.30	
15401,14 - 65	Black	11.2	16.50	
64002,261 - 114	Yellow	1.1	0.00	
64002,262 - 115	Colorless	37.4	0.00	
64002,262 - 116	Colorless	18.0	10.77	
64002,262 - 117	Black	3.0	0.00	V, Fe
64002,262 - 118	Colorless	5.0	0.00	
64002,263 - 120	Orange	1.2	66.03	
64002,263 - 122	Green	2.4	167.90	
64002,263 - 121	Black	9.0	40.84	V, Fe
64002,266 - 158	Black	13.7	27.66	V, Fe

V = vesicular
Fe = auto-reduced surface Fe mounds
L = 'lacy' Fe metal
W = Fe mounds with volatile 'waists'

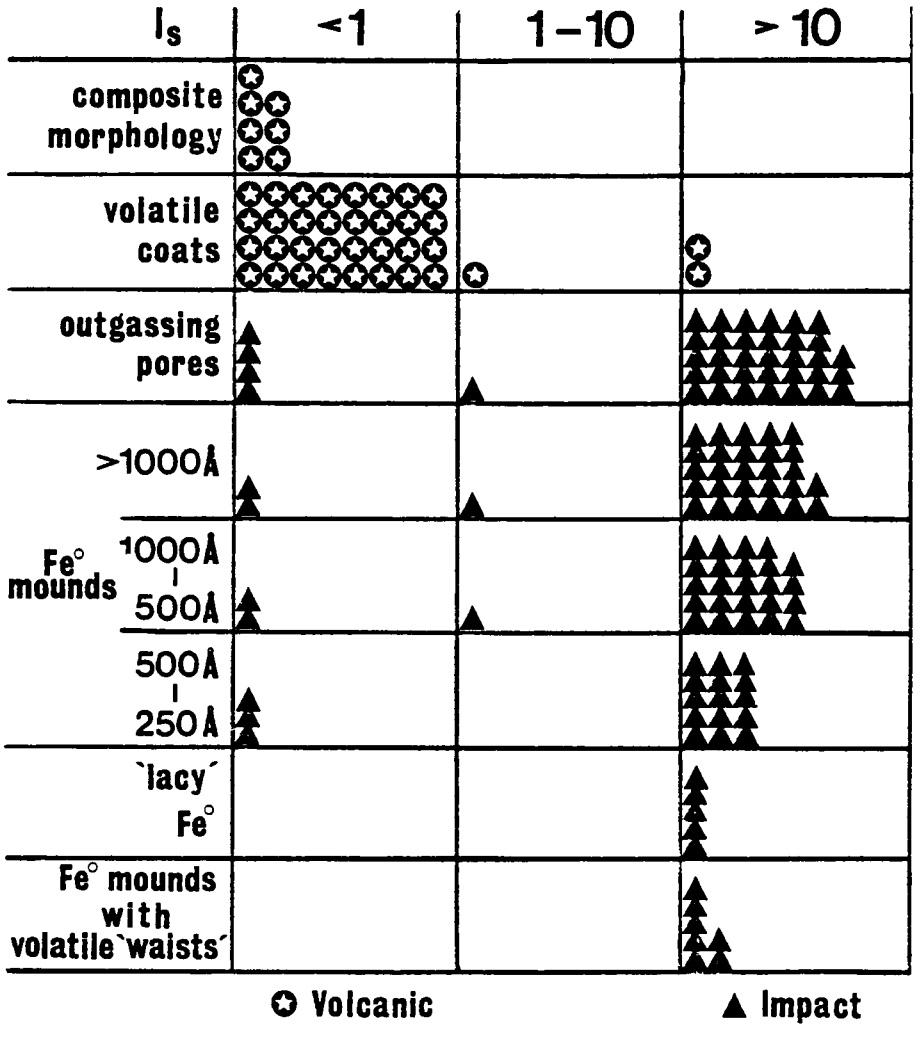


FIGURE 4. A compilation of the various diagnostic features used to determine glass bead origin and their corresponding FMR data.

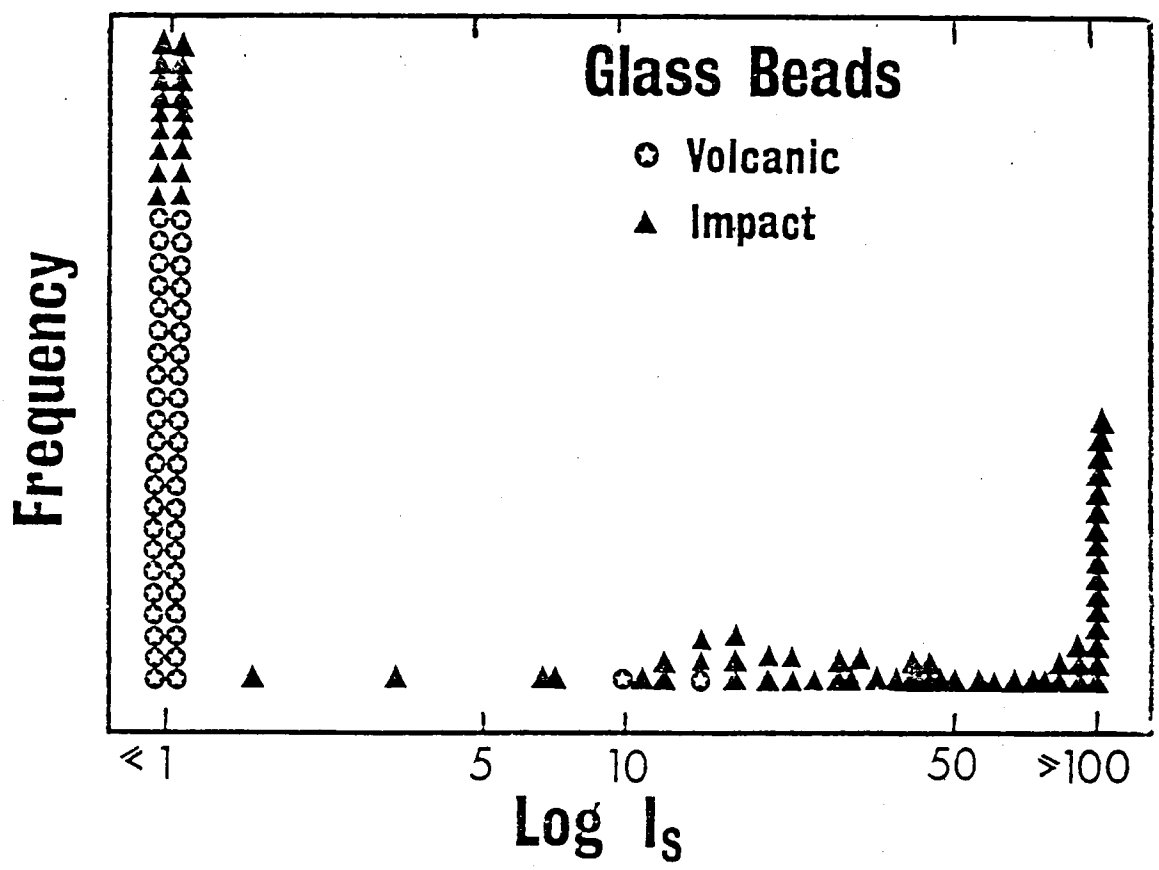


FIGURE 5. FMR data for volcanic and impact droplets shown in direct comparison.

Discussion

Delano and Livi (1981) have reported glass beads which purportedly represent 19 different volcanic compositional groups. Their recognition of these groups came through the use of many of the criteria discussed in Chapter I. However, since the beads were in thin section, SEM inspection could not be employed.

Table III summarizes all the chemical data for the volcanics in this study, and they are plotted in Figure 6. The four beads from this study which represent two other distinct compositions are additional volcanic groups. The two green, volcanic beads from 14148 are practically identical in composition to that of Delano's Apollo 14, Group C, volcanic glass (1981). The red volcanic droplets from 10084 also have compositions which approximate Apollo 11 orange volcanics (Delano and Livi, 1981). The color classification differences can be attributed to appearance of the glass when viewed as a whole sphere with a binocular microscope versus in thin section.

The lack of complete adherence to the FMR model by the impact beads could be a function of two factors. Either single-domain Fe was never produced in these beads or it was produced as a transient stage and was annealed into larger multi-domain Fe. If the beads contain little to no Fe, as in a feldspar composition, single-domain Fe would not be produced regardless of the impact history, and I_s would always be less than one. However, based on chemistry, most of the beads with near-zero I_s values contain significant FeO, as shown in Figure 7. This suggests that the primary factor responsible for the production of single domain Fe is not the FeO content of the melt. A

TABLE III

Volcanic Glass Compositions

Apollo Sample	Sample No.	SiO_2	TiO_2	Al_2O_3	Cr_2O_3	FeO	MnO	MgO	CaO	Na_2O	K_2O	TOTAL
10084,853	95	38.3	10.3	5.83	0.61	23.2	0.25	14.0	7.75	0.36	0.03	100.6
10084,853	142	38.1	9.71	5.38	0.54	23.0	0.28	15.3	7.27	0.28	0.04	99.9
14148,23	39	46.4	0.55	9.76	0.64	17.6	0.27	14.3	9.32	0.40	0.10	99.3
14148,23	40	46.5	0.59	10.1	0.55	17.5	0.21	13.9	9.44	0.31	0.09	99.2
15401,14	13	44.8	0.46	7.13	0.49	20.4	0.29	17.8	7.66	0.11	0.00	99.1
15401,14	14	44.6	0.45	7.20	0.50	20.0	0.29	17.6	8.07	0.10	0.00	98.8
15401,14	16	46.0	0.54	8.86	0.57	20.4	0.27	12.2	10.0	0.14	0.01	99.1
15401,14	68	45.8	0.41	7.25	0.41	19.7	0.24	18.3	7.95	0.13	0.03	100.2
15401,14	73	42.1	0.41	7.07	0.51	20.5	0.26	17.9	8.04	0.11	0.01	96.9
15401,14	74	43.1	0.43	7.25	0.54	20.3	0.20	18.0	8.12	0.15	0.00	98.0
15401,14	145	45.8	0.41	7.65	0.60	19.4	0.26	17.4	8.32	0.20	0.00	100.0
15401,14	146	46.4	0.39	7.65	0.55	19.3	0.21	17.3	8.32	0.22	0.00	100.3
15401,14	147	46.2	0.40	7.78	0.53	18.9	0.29	17.4	8.31	0.17	0.00	100.1
15401,14	148	46.1	0.44	7.54	0.50	19.4	0.21	17.1	8.24	0.14	0.00	100.2
74002,176	127	40.4	8.67	6.92	0.69	20.9	0.16	12.6	7.88	0.40	0.05	98.6
74002,176	129	39.9	8.71	7.02	0.62	21.0	0.21	12.9	7.87	0.48	0.07	98.8
74220,2	11	40.7	7.93	6.01	0.50	21.2	0.29	15.1	7.33	0.44	0.04	99.5
74220,6	18	40.9	9.94	7.08	0.41	20.5	0.33	11.3	9.25	0.39	0.07	100.2
74220,6	19	38.8	9.98	6.09	0.62	22.6	0.33	12.8	7.76	0.37	0.05	99.5
74220,6	97	39.0	9.02	5.79	0.63	22.5	0.25	13.3	7.27	0.34	0.05	98.0
74220,6	98	38.6	9.02	5.74	0.68	22.5	0.25	15.0	7.32	0.38	0.05	99.5
74220,6	99	38.6	8.92	5.66	0.71	22.4	0.28	15.0	7.16	0.35	0.04	99.1
74220,6	100	39.2	9.14	5.89	0.70	22.5	0.24	13.9	7.45	0.39	0.04	99.5
74220,6	101	38.6	8.81	5.52	0.73	22.0	0.21	15.2	7.11	0.38	0.07	98.5
74220,6	102	38.5	8.77	5.74	0.68	22.1	0.29	15.7	7.11	0.37	0.04	99.3
74220,6	104	38.9	8.54	5.71	0.65	21.8	0.28	15.8	6.98	0.43	0.04	99.1
74220,6	105	38.3	8.92	5.45	0.71	21.8	0.22	15.1	7.00	0.32	0.03	97.8
74220,6	106	37.8	8.89	5.50	0.65	21.5	0.36	15.6	7.06	0.36	0.03	97.7
74220,6	107	38.3	8.45	5.48	0.63	24.2	0.38	15.3	6.88	0.28	0.03	99.9
74220,6	108	38.6	8.53	5.54	0.67	24.1	0.32	15.3	6.96	0.40	0.02	100.4
74220,6	109	39.0	8.64	5.69	0.62	23.5	0.33	15.7	7.05	0.32	0.04	100.8
74220,6	110	38.4	8.53	5.63	0.64	23.5	0.32	15.5	6.89	0.39	0.04	99.9
74220,6	111	38.4	8.79	5.71	0.71	23.6	0.29	14.8	7.08	0.34	0.05	99.7
74220,6	112	38.4	8.80	5.88	0.70	23.5	0.29	15.5	7.07	0.32	0.06	100.4

FIGURE 6. Plot of volcanic and impact beads with $I_s < 1$. "Other" volcanics are shown with sample numbers. The impact beads are shown in the fields defined by cluster analysis techniques by other investigators and are labelled by the rock type they were derived from.

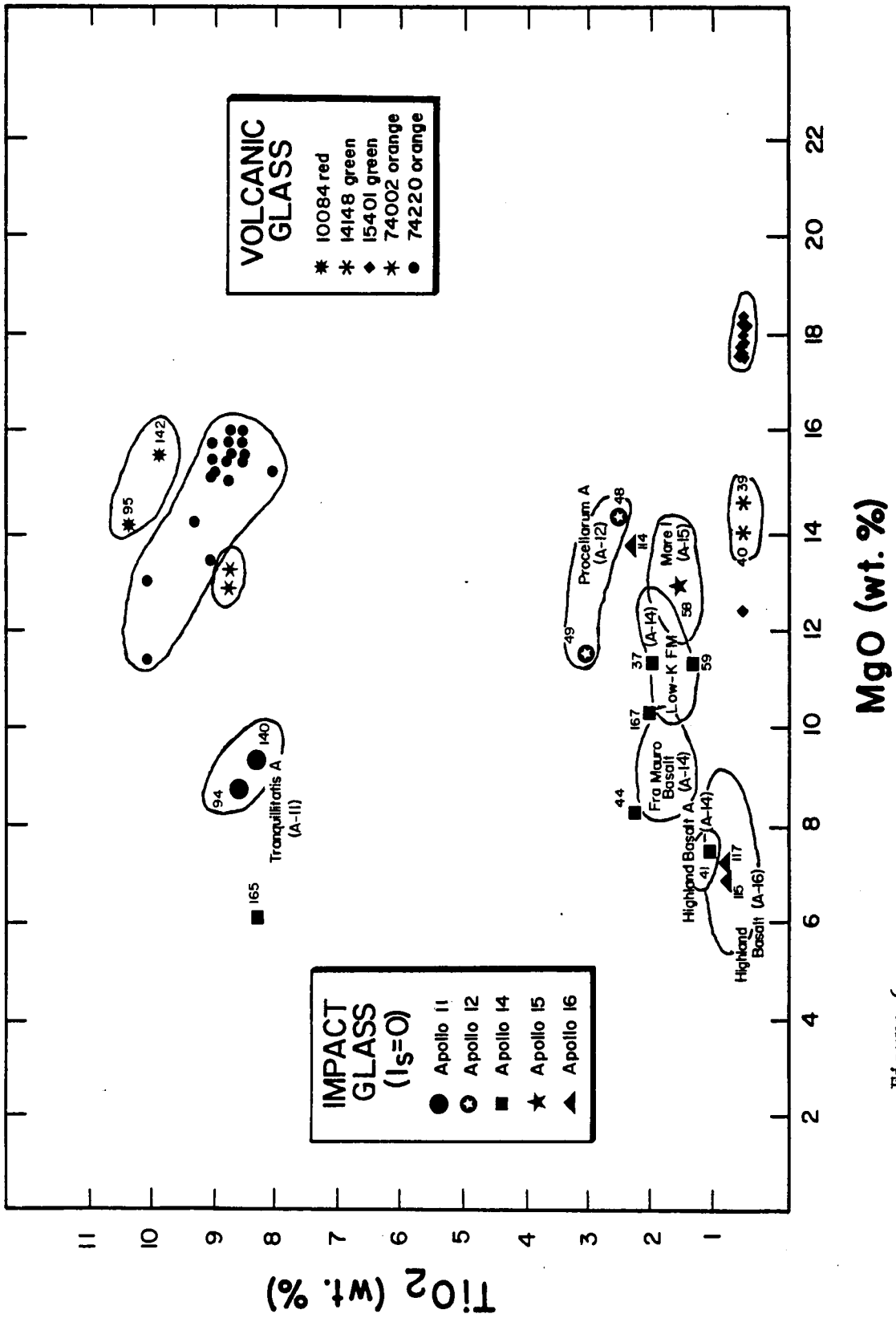

VOLCANIC GLASS
10084 red
14148 green
15401 green
74002 orange
74220 orange
IMPACT GLASS (Is=0)
Apollo 11
Apollo 12
Apollo 14
Apollo 15
Apollo 16
Tranquillitatis A (A-11)
Procellarum A (A-12)
Fra Mauro Basalt A (A-14)
Low-K FM (A-14)
Mare I (A-15)
Highland Basalt (A-14)
Highland Basalt (A-16)
TiO2 (wt. %)
MgO (wt. %)

Figure 6.

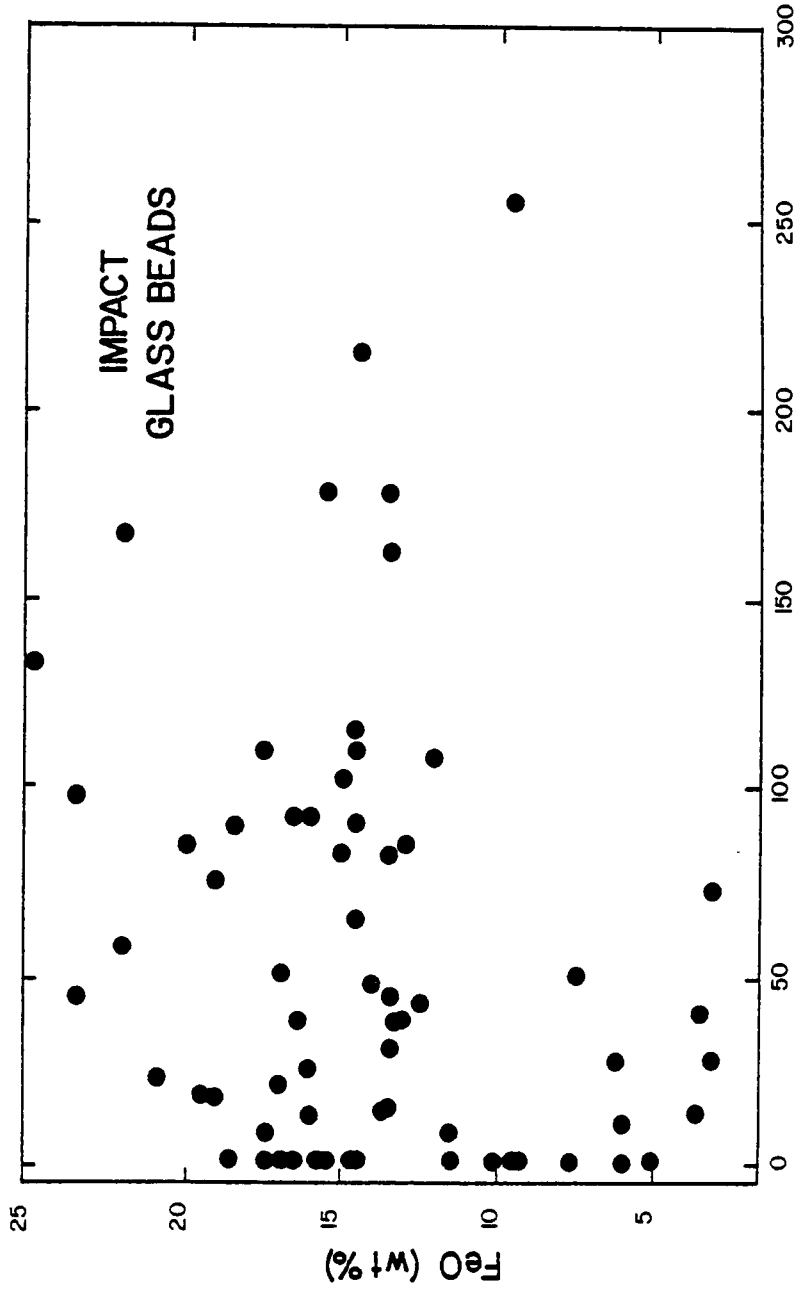


FIGURE 7. FeO vs I_s for all impact beads in this study.

summary of additional impact glass chemistry is presented in Table IV.

If the impact producing the bead formed its melt principally from bedrock which lacks solar-wind implanted hydrogen and carbon (Kaplan et al., 1970; Friedman et al., 1971; DesMarais, 1974), the Fe^{2+} in the melt would undergo only a negligible amount of reduction, and little single-domain Fe would result (i.e., I_s would remain low). Similarly, a large impact might be expected to produce a large ejecta cloud in which individual glass droplets would lose heat more slowly compared to a small ejecta cloud. This would occur because the cloud itself must lose heat to its surroundings before individual droplets can cool. Consequently, droplets in a large cloud would be more likely to anneal their single-domain Fe into larger, multi-domain Fe with a subsequent loss of I_s. Also, large impacts are more likely to penetrate completely through the regolith and melt underlying bedrock, compared to small impacts. Large impacts should favor low I_s which should be mostly associated with bedrock-derived melt. Small impacts would favor high I_s because the beads will be derived from near the surface with large proportions of solar-wind saturated regolith. Cooling would also occur more quickly.

Chemical data from the impact glasses with I_s levels of zero illustrate the tendency of these beads to reflect bedrock compositions. Cluster analysis techniques of glass beads performed in other studies (Reid et al., 1972a.; 1972b; Ridley et al., 1973; Warner et al., 1979) found groupings of preferred compositions which were related to rock

TABLE IV

Impact Glass Compositions

Apollo Sample	Sample NO.	SiO_2	TiO_2	Al_2O_3	Cr_2O_3	FeO	MnO	MgO	CaO	Na_2O	K_2O	TOTAL
10011,11	76	39.6	6.66	14.9	0.26	16.8	0.16	7.56	12.5	0.39	0.07	98.9
10084,853	4	41.0	10.0	9.29	0.18	19.2	0.17	8.50	10.9	0.25	0.09	99.6
10084,853	5	42.0	6.40	14.9	0.13	13.7	0.21	8.46	12.2	0.11	0.04	98.1
10084,853	6	40.1	6.69	15.1	0.11	13.5	0.18	8.83	12.7	0.06	0.04	97.3
10084,853	7	42.6	6.90	9.71	0.17	18.5	0.27	8.25	11.9	0.14	0.07	98.4
10084,853	8	44.0	2.44	17.6	0.26	13.1	0.18	7.70	12.5	0.32	0.03	98.1
10084,853	77	37.7	8.39	12.5	0.37	16.5	0.27	8.09	11.4	0.34	0.12	95.6
10084,853	78	44.5	6.09	13.0	0.33	14.6	0.20	9.25	12.8	0.32	0.10	101.1
10084,853	79	40.1	7.52	9.09	0.36	24.8	0.26	6.69	10.9	0.25	0.13	100.3
10084,853	80	39.9	7.29	15.1	0.25	15.8	0.09	7.55	12.3	0.28	0.08	98.6
10084,853	82	42.1	7.16	12.3	0.34	15.6	0.20	8.12	11.8	0.20	0.06	97.9
10084,853	84	42.9	3.76	14.3	0.33	13.5	0.09	13.7	10.1	0.18	0.02	98.8
10084,853	86	43.7	4.00	13.8	0.36	13.7	0.17	13.7	9.80	0.22	0.03	99.6
10084,853	90	40.9	9.81	10.3	0.33	17.7	0.25	8.72	11.5	0.14	0.02	99.7
10084,853	94	38.6	8.45	15.1	0.13	15.3	0.25	8.68	12.9	0.01	0.02	99.4
10084,853	95	38.3	10.3	5.83	0.61	23.2	0.25	14.0	7.75	0.36	0.03	100.6
10084,853	137	42.8	6.59	14.4	0.24	14.3	0.20	8.03	12.3	0.16	0.06	99.1
10084,853	138	40.7	5.70	18.3	0.22	12.0	0.19	8.25	13.7	0.04	0.01	99.1
10084,853	140	36.1	8.18	16.7	0.21	14.4	0.17	9.10	14.0	0.03	0.00	98.8
10084,853	143	37.3	7.42	15.7	0.18	14.8	0.18	9.16	13.5	0.00	0.00	98.2
10084,853	149	38.0	7.95	16.1	0.21	14.7	0.18	9.24	13.5	0.05	0.00	99.8
10084,853	150	46.4	4.27	12.3	0.23	12.9	0.16	12.4	11.0	0.33	0.05	100.0
10084,853	151	38.4	6.73	4.25	0.60	23.6	0.29	22.1	4.30	0.47	0.20	100.9
10084,853	152	37.3	9.90	5.71	0.63	23.4	0.25	15.0	7.46	0.43	0.02	100.0
10084,853	153	42.2	6.77	15.2	0.25	14.4	0.23	8.73	12.2	0.33	0.09	100.5
12001,7	3	46.4	2.77	11.3	0.41	17.7	0.18	11.6	9.79	0.27	0.07	100.4
12001,7	23	46.2	2.97	14.9	0.13	13.0	0.16	9.99	11.0	0.12	0.08	98.5
12001,7	47	45.3	1.96	10.1	0.49	14.1	0.27	12.3	11.1	0.35	0.09	96.1
12001,7	48	40.8	2.48	13.7	0.27	17.6	0.19	14.3	9.59	0.01	0.00	98.9
12070,29	50	44.2	2.94	13.1	0.31	16.3	0.21	11.1	10.6	0.07	0.04	98.8
12070,29	51	46.7	1.82	16.6	0.26	13.3	0.19	8.19	10.8	1.05	0.46	99.4

TABLE IV (continued)

Apollo Sample	Sample NO.	SiO_2	TiO_2	Al_2O_3	Cr_2O_3	FeO	MnO	MgO	CaO	Na_2O	K_2O	TOTAL
12070,104	1	43.0	2.97	13.5	0.25	16.9	0.20	12.7	10.8	0.05	0.03	100.3
12070,104	49	41.7	3.10	15.5	0.23	15.3	0.19	11.4	11.7	0.02	0.00	99.1
12070,104	53	45.1	2.52	12.8	0.40	15.8	0.23	9.74	10.2	0.18	0.07	97.1
12070,104	55	44.7	0.26	26.8	0.05	3.64	0.03	7.09	15.7	0.12	0.01	98.4
12070,104	154	46.6	2.62	15.7	0.29	13.4	0.18	9.50	10.5	0.39	0.16	99.5
12070,104	156	45.1	0.64	22.6	0.10	7.60	0.14	9.93	11.9	0.16	0.04	98.2
12070,104	157	41.1	3.18	16.0	0.25	15.9	0.23	11.6	12.5	0.05	0.00	100.7
12070,104	52	46.3	1.57	18.7	0.16	9.71	0.07	10.2	11.3	0.14	0.09	98.2
14003,28	63	48.1	0.19	16.9	0.38	6.11	0.09	19.7	9.54	0.07	0.01	101.0
14141,30	36	45.3	1.56	15.9	0.21	11.5	0.11	11.1	9.78	0.32	0.22	96.0
14141,30	44	48.4	2.16	14.6	0.17	11.4	0.22	8.13	10.2	0.63	0.53	96.4
14141,30	165	44.2	8.29	10.5	0.10	18.5	0.31	6.01	10.9	0.85	0.18	99.8
14141,23	34	45.4	3.66	14.8	0.05	12.5	0.13	9.32	9.98	0.66	0.47	97.0
14141,23	35	41.3	7.57	12.6	0.30	15.0	0.16	10.6	9.25	0.50	0.25	97.5
14148,23	37	40.7	1.95	21.2	0.00	9.46	0.13	11.3	13.5	0.02	0.03	98.3
14148,23	41	45.4	0.97	21.7	0.16	7.64	0.12	7.45	13.0	0.59	0.32	97.3
14148,23	163	41.5	3.14	11.9	0.32	20.0	0.29	11.7	10.0	0.14	0.02	99.0
14149,39	164	48.7	0.52	29.3	0.02	3.02	0.07	2.61	14.6	1.96	0.41	101.2
14156,23	59	46.3	1.13	18.9	0.20	9.68	0.14	11.2	10.5	0.92	0.24	99.2
14156,23	62	42.6	4.79	15.1	0.38	13.4	0.22	9.69	11.7	0.14	0.02	98.0
14156,23	167	43.5	1.97	20.0	0.12	10.0	0.08	10.3	12.3	0.06	0.04	98.3
14156,23	168	44.6	2.99	11.3	0.35	21.2	0.27	8.55	10.7	0.05	0.04	100.0
15401,14	57	42.5	3.67	8.53	0.57	21.9	0.29	12.6	8.41	0.48	0.07	99.0
15401,14	58	43.3	1.48	14.9	0.30	14.5	0.22	12.8	11.2	0.06	0.01	98.7
15401,14	64	45.9	0.43	7.94	0.63	19.3	0.27	17.2	8.29	0.13	0.01	100.1
15401,14	65	45.6	0.42	7.34	0.47	19.2	0.25	16.8	8.45	0.09	0.03	98.7
64002,261	114	47.6	2.36	9.11	0.27	16.9	0.25	13.6	8.37	0.38	0.09	99.0
64002,262	115	40.1	0.63	28.5	0.04	5.24	0.03	6.75	16.4	0.03	0.00	97.7
64002,262	116	43.5	0.18	25.0	0.14	5.75	0.08	8.73	13.8	0.36	0.04	97.6
64002,262	117	44.4	0.66	26.3	0.15	6.04	0.06	7.29	14.9	0.40	0.09	100.3
64002,262	118	42.5	0.24	13.2	0.40	16.4	0.26	18.3	8.02	0.84	0.04	100.2
64002,263	120	43.3	6.25	14.1	0.41	14.5	0.18	10.1	11.6	0.05	0.01	100.6
64002,263	122	43.5	0.39	7.80	0.47	21.8	0.23	17.3	8.30	0.14	0.00	99.9
64002,264	121	43.4	0.30	29.8	0.09	3.36	0.00	3.69	16.7	0.34	0.05	97.7
64002,266	158	44.8	0.34	30.1	0.04	3.02	0.07	4.15	16.8	1.10	0.10	100.6

types. The impact glasses in this study with $I_s < 1$ correspond closely to several compositional groupings reported by the other investigators. Figure 7 and Table V present data of the impact glasses in this study and are compared to the established groups. As can be seen, most of the compositions from the present statistical compilation plot within clusters of those previously delineated.

Impact-derived beads may originate in the regolith, in lunar bedrock beneath the regolith, or may contain material from each. FMR data may reflect this origin. No clear criteria have been established for distinguishing among these origins. Delano et al. (1981) show that most glass beads, when plotted as ratios of refractory elements so as to minimize effects of vapor fractionation, fall on mixing curves between highland and mare rock types. They conclude that most beads were made from mixed regolith of various intermediate compositions. However, this chemical technique probably cannot distinguish between mixing which originates in a regolith and mixing caused by a large cratering event sampling different types and proportions of bedrock. An example is a large crater which completely penetrates a mare basalt flow and excavates highland bedrock beneath. Some of the impact melt from this event may be mixtures of melted basalt and melted highland bedrock. Layers of pyroclastic volcanics also could be sampled by such an event. The resulting mixed melt conceivably could have a composition identical to some parts of the overlying regolith which can also be a source of impact-glass beads. Consequently, chemical criteria may not be diagnostic of the source of the impact glass.

TABLE V

Impact Glass Chemical Compositions Compared to Previously Reported Bedrock-Derived Glass Compositions

	Tranquillitatis A[a]	10084 (94)	10084 (140)	Procellarum A[a]	12001 (48)	12070 (49)	Highland[a] Basalt A	14148 (41)
SiO_2	40.2	38.6	36.1	43.7	40.8	41.7	45.3	44.1
TiO_2	7.2	8.45	8.18	3.3	2.48	1.96	0.4	.73
Al_2O_3	13.2	15.1	16.7	13.2	13.7	8.42	25.8	21.7
FeO	16.5	15.3	14.4	16.5	17.6	14.9	5.6	7.64
MgO	8.5	8.68	9.10	9.9	14.3	10.6	7.9	7.45
CaO	12.0	12.9	14.0	11.1	9.59	11.7	14.8	13.0
Na_2O	0.30	0.01	0.03	0.2	0.03	0.02	0.2	0.59
K_2O	0.10	0.02	0.00	0.16	0.01	0.00	0.07	0.32

	low-K Fra Mauro[b]	14148 (37)	14156 (167)	Fra Mauro[a] Basalt	14148 (44)	Mare 1[b]	15401 (58)	Highland[c] Basalt	64002 (117)
SiO_2	46.6	40.7	43.5	48.0	48.4	45.7	43.3	45.4	44.4
TiO_2	1.25	1.95	1.97	2.1	2.16	1.6	1.48	0.43	0.66
Al_2O_3	18.8	21.2	20.0	17.0	14.6	13.3	14.9	27.6	26.3
FeO	9.67	9.46	10.0	10.9	11.4	15.8	14.5	4.62	6.04
MgO	11.0	11.3	10.3	8.7	8.13	11.7	12.8	6.13	7.29
CaO	11.6	13.5	12.3	10.7	8.13	10.4	11.2	15.6	14.9
Na_2O	0.37	0.02	0.06	0.70	0.63	0.30	0.06	0.42	0.40
K_2O	0.12	0.03	0.04	0.54	0.53	0.10	0.01	0.05	0.09

a. Reid et al., 1972a
b. Reid et al., 1972b
c. Ridley et al., 1973

CHAPTER VI

CONCLUSION

The intensity of ferromagnetic resonance (I_s) was tested for potential use as an additional criterion to be used in distinguishing volcanic glass spherules from particles produced through impact processes. This method is capable of detecting single-domain Fe metal formed only during impact process.

Scanning electron microscopy, proven to be the most definitive method of establishing a glass bead's mode of origin, was used as a foundation upon which to correlate FMR data and thereby test the FMR as criterion. Characteristic surface features on "type" volcanic spherules were used for recognition of other volcanic particles and discrimination from impact-produced beads.

Results from the data show that 94% of the volcanic spherules had values of I_s less than one. Of the impact beads, 75% had values of I_S greater than one. The I_S values for the impact beads may provide a criterion for distinguishing regolith-derived beads from bedrock-derived beads. However, this application of the criterion has yet to be tested. By analogy with the volcanic beads, it is necessary to use "type" regolith-derived impact glass and "type" bedrock-derived impact glass. The agglutinates analyzed during the course of this study have relatively high I_s and can qualify as "type" impact glass. The ropy glasses described by Fruland et al. (1977) could possibly be considered as "type" bedrock-derived glass candidates, though no systematic FMR data now exists for these particles. However, using

chemical data previously reported, the correlation of bedrock-derived compositions with impact glasses from this study having I_s values less than one are good and seem to substantiate the recognition of bedrock-derived impact glasses as an additional use for the FMR method.

With the demonstration that the I_s value of a glass bead can be a reliable, non-destructive basis for a new criterion used for the recognition of a glass bead's genesis, comes the additional benefit of its use on glass fragments. The lack of original, primary surfaces on glass beads would render SEM inspection useless in the attempt to discern their mode or origin. The intrinsic magnetic signatures of such fragments would probably remain intact and allow the FMR method to aid greatly in the screening procedure for genesis determination.

The actual procedure is a simple one. A glass bead or fragment is placed in the EPR spectrometer. Two spectra, requiring a total of 16 minutes to generate, indicate the FMR absorption intensity (I_s). An I_s value greater than one suggests the bead has resulted from an impact process with regolith involvement. An I_s value less than one indicates the lack of single-domain Fe metal. These beads could have been produced by volcanic fire-fountaining and will reflect relatively primary magma compositions. Beads with I_s values less than one may also represent glasses produced by impact melting of bedrock by large cratering events. These could be significant samples considering that they may be the only material collected from otherwise unsampled rock types. Both of these glass types are valuable and further inspections by the SEM should be used to confirm their genesis.

Ultimately, this technique could contribute to the augmentation of the present collection of volcanic- and bedrock-glass compositions. Since the glass beads in the lunar soils are so widely distributed, they provide a glimpse of material which originated from areas distant to the landing sites and are otherwise unattainable.

LIST OF REFERENCES

LIST OF REFERENCES

Adams, J. B., Pieters C., and McCord, T. B., Orange glass: evidence for regional deposits of pyroclastic origin on the Moon, Proc. Lunar Sci. Conf. 5th, p. 171-186, 1974.

Agrell, S. O., Scoon J. H., Muir I. D., Long J. V. P., McConnell J. D. C., and Peckett A., Observations on the chemistry, mineralogy, and petrology of some Apollo 11 lunar samples, Proc. Apollo 11 Lunar Sci. Conf., p. 93-128, 1970.

Agrell, S. O., Agrell J. E., Arnold A. R., and Bristol C. C., Observations on glass from 15425, 15426, 15427 (abstract), in Lunar Science IV, Lunar Science Institute, Houston, p. 12-14, 1973.

Albee, A. C. and Ray, L., Correction factors for electron-probe microanalysis of silicates, oxides, carbonates, phosphates, and sulphides, Anal. Chem. 42, p. 1408-1414, 1970.

Basu, A. and Bower, J. F., Provenance of Apollo 15 deep drill core sediments, Proc. Lunar Sci. Conf. 8th, p. 2841-2867, 1977.

Bell, P. M., Goresy, A. El, and Mao, H. K., A study of iron-rich particles on the surfaces of orange glass spheres from 74220, Proc. Lunar Sci. Conf. 5th, p. 187-191, 1974.

Bence, A. E. and Albee, A. C., Empirical correction factors for the electron microanalysis of silicates and oxides, Jour. of Geol. 76, p. 382-403, 1968.

Butler, P., Jr. and Meyer, C., Jr., Sulphur prevails in coatings on glass droplets: Apollo 15 green and brown glasses and Apollo 17 orange and black (devitrified) glasses, Proc. Lunar Sci. Conf. 7th, p. 1561-1581, 1976.

Carter, J. L., Chemistry and surface morphology of fragments from Apollo 12 soil, Proc. Lunar Sci. Conf. 2nd, p. 873-892, 1971.

Carter, J. L., Morphology and chemistry of probable VLS (Vapor-Liquid-Solid) type of whisker structures and other features on the surface of breccia 15015, 36, Proc. Lunar Sci. Conf. 4th, p. 413-421, 1973.

Carter, J. L. and McKay, D. S., Metallic mounds produced by reduction of material of simulated lunar composition and implications on the origin of metallic mounds on lunar glasses, Proc. Lunar Sci. Conf. 3rd, p. 953-970, 1972.

Carter, J. L., Taylor, H. C. J., and Padovani, E., Morphology and chemistry of particles from Apollo 17 soils 74220, 74241 and 75081, Trans. Amer. Geophys. Union 54, p. 582-584, 1973.

Cavaretta, G., Coradini, A., Funiciello, R., Fulchignoni, M., Tadeuci, A., and Trigila, R., Glassy particles in Apollo 14 soil 14163, 88: Peculiarities and genetic considerations, Proc. Lunar Sci. Conf. 3rd, p. 1085-1094, 1972.

Chang, S., Mack, R., Gibson, E. K., Jr., and Moore, G. W., Simulated solar wind implantation of carbon and nitrogen ions into terrestrial basalt and lunar fines, Proc. Lunar Sci. Conf. 4th, p. 1509-1522, 1973.

Chou, C. L., Boynton, W. V., Sundberg, L. L., and Wasson, J. T., Volatiles on the surface of Apollo 15 green glass and trace-element distributions among Apollo 15 soils, Proc. Lunar Sci. Conf. 6th, p. 1701-1727, 1975.

Clanton, U.S., McKay, D. S., and Ladle, G. H., Scanning electron microscopy of lunar material, JEOL News 11, no. 2, p. 2-9, 1973.

Clanton, U.S., McKay, D. S., Waits, G., and Fuhrman, R., Sublimate morphology on 74001 and 74002 orange and black glassy droplets, Proc. Lunar Planet Sci. Conf. 9th, 1945-1957, 1978.

Delano, J. W., Major element composition of volcanic green glasses from Apollo 14, Lunar and Planetary Science XII, p. 217-219, Lunar and Planetary Institute, Houston, TX, 1981.

Delano, J. W. and Livi, K., Lunar volcanic glasses and their constraints on mare petrogenesis, Geochim et Cosmochim Acta 45, p. 2137-2149, 1981.

Delano, J. W., Lindsley, D. H., and Rudowski, R., Glasses of impact origin from Apollo 11, 12, 15 and 16: Evidence for fractional vaporization and mare/highland mixing, Proc. Lunar Planet Sci. Conf. 12th, p. 339-370, 1981.

Eberhardt, P., Geiss, J., Graf, H., Grogler, N., Mendia, M. D., Morgeli, M., Schwaller, H., and Stettler, A., Trapped solar wind noble gases in Apollo 12 lunar fines 12001 and Apollo 111 beccia 10046, Proc. Lunar Sci. Conf. 3rd, p. 1821-1856, 1972.

Fruland, R. M., Morris, R. V., McKay, D. S., and Clanton, U.S., Apollo 17 ropy glasses, Proc. Lunar Sci. Conf. 8th, p. 3095-3111, 1977.

Goldstein, J. I., Henderson, E. P. and Yakowitz, H., Investigation of lunar metal particles, Proc. Apollo 11 Lunar Sci. Conf., p. 499-512, 1970.

Goldstein, J. I. and Axon, H. J., Composition, structure and thermal history of metallic particles from 3 Apollo soils, 65701, 68501, 63501, Proc. Lunar Sci. Conf. 4th, p. 751-775, 1973.

Goldstein, J. I., Hewins, R. H., and Axon, H. J., Metal silicate relationships in Apollo 17 soils, Proc. Lunar Sci. Conf. 5th, p. 653-671, 1974.

Haggerty, S. E., Apollo 17 orange glass: Textural and morphological characteristics of devitrification, Proc. Lunar Sci. Conf. 5th, p. 207-222, 1972.

Head, J. W., Lunar dark-mantle deposits: Possible clues to the distrubution of early mare deposits, Proc. Lunar Sci. Conf. 5th, p. 207-222, 1974.

Heiken, G. A. (compiler), A Catalogue of Lunar Soils, 221 pp., LBJ Space Center, NASA, Houston, TX, 1974.

Heiken, G. A., Petrology of Lunar Soils, Reviews of Geophys. and Space Phys., vol. 13, no. 4, p. 567-587, 1975.

Heiken, G. A. and McKay, D. S., Petrography of Apollo 17 soils, Proc. Lunar Sci. Conf. 5th, p. 843-860, 1974.

Heiken, G. A. and McKay, D. S., A model for eruption behavior of a volcanic vent in eastern Mare Serenitatis, Proc. Lunar Sci. Conf. 8th, p. 3243-3255, 1977.

Housley, R. M., Modelling lunar volcanic eruptions, Proc. Lunar Planet Sci. Conf. 9th, p. 1473-1484, 1978.

Housley, R. M., Blander, M., Abdel-Gawad, M., Grant, R. W., and Muir, A. H., Jr., Mossbauer spectroscopy of Apollo 11 samples, Proc. Apollo 11 Lunar Sci. Conf., p. 2251-2268, 1970.

Housley, R. M., Grant, R. W., and Abdel-Gawad M., Study of excess Fe metal in the lunar fines by magnetic separation, Mossbauer spectroscopy, and microscopic examination, Proc. Lunar Sci. Conf. 3rd, p. 1065-1076, 1972.

Housley, R. M., Grant, R. W., and Paton, N. E., Origin and characteristics of excess Fe metal in lunar glass welded aggregates, Proc. Lunar Sci. Conf. 4th, p. 2737-2749, 1973.

Housley, R. M., Cirlin, E. H., Paton, N. E., and Goldberg, I. B., Solar wind and micrometeorite alteration of the lunar regolith, Proc. Lunar Sci. Conf. 5th, p. 2623-2642, 1974.

Housley, R. M., Cirlin, E. H., Goldberg, I. B., and Crowe, H., Ferromagnetic resonance studies of lunar core stratigraphy, Proc. Lunar Sci. Conf. 7th, p. 13-26, 1976.

Huneke, J. C., Jessberger, E. K., and Wasserburg, G. J., The age of metamorphism of a highland breccia (65015) and a glimpse at the age of its protolith (abstract), Lunar Science V, p. 375-377, Lunar Science Institute, Houston, TX, 1974.

Keil, K., Kurat, G., Prinz, M., and Green, J. A., Lithic fragments, glasses and chondrules from Luna 16 finds, Earth and Planet Sci. Letters 13, p. 243-256, 1971.

Ladle, G. H., Scanning electron microscopy and petrography of glassy particles produced by lava fountain eruptions (Ph.D. dissertation, Brigham Young Univ.), Lunar and Planetary Institute Contribution No. 325, Houston, TX, 1978.

Lucchita, B. K. and Schmitt, H. H., Orange material in the Sulpicius Gallus Formation at the southwestern edge of Mare Serenitatis, Proc. Lunar Sci. Conf. 5th, p. 223-234, 1974.

McKay, D. S. and Heiken, G. A., Petrology and scanning electron microscope study of Apollo 17 orange and black glass, Trans. Amer. Geophys. Union 54, p. 599-600, 1973.

McKay, D. S., Heiken, G. A., Taylor, R. M., Clanton, U.S., Morrison, D. A., and Ladle, G. H., Apollo 14 soils: Distribution and particle size, Proc. Lunar Sci. Conf. 3rd, p. 983-994, 1972.

McKay, D. S., Clanton, U. S., and Ladle, G. H., Scanning electron microscope study of Apollo 15 green glass, Proc. Lunar Sci. Conf. 4th, p. 225-238, 1973.

McKay, D. S., Fruland, R. M., and Heiken, G. H., Grain size and evolution of lunar soils, Proc. Lunar Sci. Conf. 5th, p. 887-906, 1974.

Mehta, S. and Goldstein, J. I., Analytical electron microscopy study of submicroscopic metal particles in glassy constituents of 15015 and 60095 lunar breccias (abstract) in Lunar and Planetary Science X, p. 816-818, 1979.

Meyer, C., Jr., McKay, D. S., Anderson, D. H., and Butler, P., Jr., The source of sublimates on the Apollo 15 green and Apollo 17 orange glass samples, Proc. Lunar Sci. Conf. 7th, p. 1673-1699, 1975.

Morris, R. V., Surface exposure indices of lunar soils: A comparative FMR study, Proc. Lunar Sci. Conf. 7th, p. 315-335, 1976.

Morris, R. V., In situ reworking (gardening) of the lunar surface: evidence from the Apollo cores, Proc. Lunar Planet Sci. Conf. 9th, p. 1801-1811, 1978b.

Morris, R. V., The surface exposure (maturity) of lunar soils: Some concepts and I_s/FeO compilation, Proc. Lunar Planet Sci. Conf. 9th, p. 2287-2297, 1978.

Morris, R. V., FMR and magnetic studies of Luna 24 soils and <1mm soil particles, in Mare Crisum: The View from Luna 24, p. 117-123, 1978c.

Morris, R. V., Origin and size distribution of metallic iron particles in the lunar regolith, Proc. Lunar Planet Sci. Conf. 11th, p. 1697-1712, 1980.

Morris, R. V. and Gose, W. A., Depositional history of core section 74002; Depth profile of maturity, FeO, and metal, Proc. Lunar Sci. Conf. 8th, p. 3115-3122, 1977.

Morris, R. V., Gose, W. A., and Lauer, H. V., Jr., Depositional and surface exposure history of the Shorty Crater core 74001/2: FMR and magnetic studies, Proc. Lunar Planet Sci. Conf. 9th, p. 2033-2048, 1978.

Muller, O., Solar wind nitrogen and indigneous nitrogen in Apollo 17 lunar samples, Proc. Lunar Sci. Conf. 5th, pp. 1907-1918, 1974.

Norman, M., Coish, R. A., and Taylor, L. A., Glass chemistry and magma evolution at Mare Crisium, in Papers Presented to the Conference on Luna 24, p. 136-139, 1977.

Norman, M., Coish, R. A., and Taylor, L. A., Glasses in the Lunar 24 core and petrogenesis of ferrobasalts, in Mare Crisium: The View from Luna 24, Pergammon Press, p. 281-289, 1978.

Papanastassiou, D. A. and Wasserburg, G. J., Rb-Sr ages and initial strontium in Apollo 15 basalts, Earth Planet Sci. Lett. 17, p. 324-337, 1973.

Pieters, C., McCord, T. B., Zisk, S., and Adams, J. B., Lunar black spots and nature of the Apollo landing area, Jour. of Geophys. Research 78, no. 26, p. 5867-5875, 1973.

Prinz, M., Dowty, E., and Keil, K., A model for the origin of orange and green glasses and the filling of mare basins, Trans. Amer. Geophys. Union 54, p. 605, 1973.

Reid, A. M., Warner, J., Ridley, W. I., Johnston, D. A., Harmon, R. S., Jakes, P., and Brown, R. W., The major element compositions of lunar rocks as inferred from glass compositions in the lunar soils, Proc. Lunar Sci. 3rd, p. 363-378, 1972a.

Reid, A. M., Warner, J., Ridley, W. I., and Brown, R. W., Major element composition of glasses in three Apollo 15 soils, Meteorites 17, no. 3, p. 395-415, 1972b.

Roedder, E. and Weiblen, P. W., Origin of orange glass spherules in Apollo 17 sample 74220, Trans. Amer. Geophys. Union 54, p. 612-613, 1973.

Runcorn, S. R., Collinson, D. W., O'Reilly, W., Battey, M. H., Stephenson, A., Jones, J. M., Manson, A. J., and Readman, P. W., Magnetic properties of Apollo 11 Lunar Samples, Proc. Apollo 11 Lunar Sci. Conf., p. 2369-2387, 1970.

Schaeffer, O. A. and Husain, L., Isotopic ages of Apollo 17 lunar material (abstract), Trans. Amer. Geophys. Union 54, p. 614, 1973.

Simonds, C. H., Warner, J. L., McGhee, P. E., Chochran, A., and Brown, R. W., Luna 24: Petrogenetic potpourri (abstract), in Papers Presented to the Conference on Luna 24, Lunar Science Institute, Houston, TX, p. 170-173, 1977.

Solomon, S. C. and Head, J. W., Vertical movement in Mare basins: Relation to mare emplacement, basin tectonics and lunar thermal history, Jour. of Geophys. Research 84, no. B4, p. 1667-1682, 1979.

Stone, C. D., and Taylor, L. A., Ferromagnetic resonance as a determinant for origin of lunar glass beads (abstract), Lunar and Planetary Science XIII, Lunar and Planetary Science Institute, Houston, TX, p. 774-775, 1982a.

Stone, C. D. and Taylor, L. A., Lunar glass beads: A comparison of SEM, FMR (I_s), and compositional features (abstract), Lunar and Planetary Science XIII, Lunar and Planetary Science Institute, Houston, TX, p. 776-777, 1982b.

Tera, F., Papanastissious, D. A., and Wasserburg, G. J., Isotopic evidence for a terminal lunar cataclysm, Earth Planet Sci. Lett. 22, p. 1-21, 1974.

Warner, R. D., Taylor, J. G., and Keil, K., Composition of glasses in Apollo 17 samples and their relation to known lunar rock types, Proc. Lunar Planet Sci. Conf. 10th, p. 1437-1456, 1979.

Wasson, J. T., Boynton, W. V., Kallemeyer, G. W., Sundberg, L. L., and Chien, M. W., Volatile compounds released during lunar lava fountaining, Proc. Lunar Sci. Conf. 7th, p. 1583-1595, 1976.

Wolfe, E. W., Lucchita, B. K., Reed, U.S., Ulrich, G. E., and Sanchez, A. G., Geology of the Taurus-Littrow Valley floor, Proc. Lunar Sci. Conf. 6th, p. 2463-2482, 1975.

APPENDICES

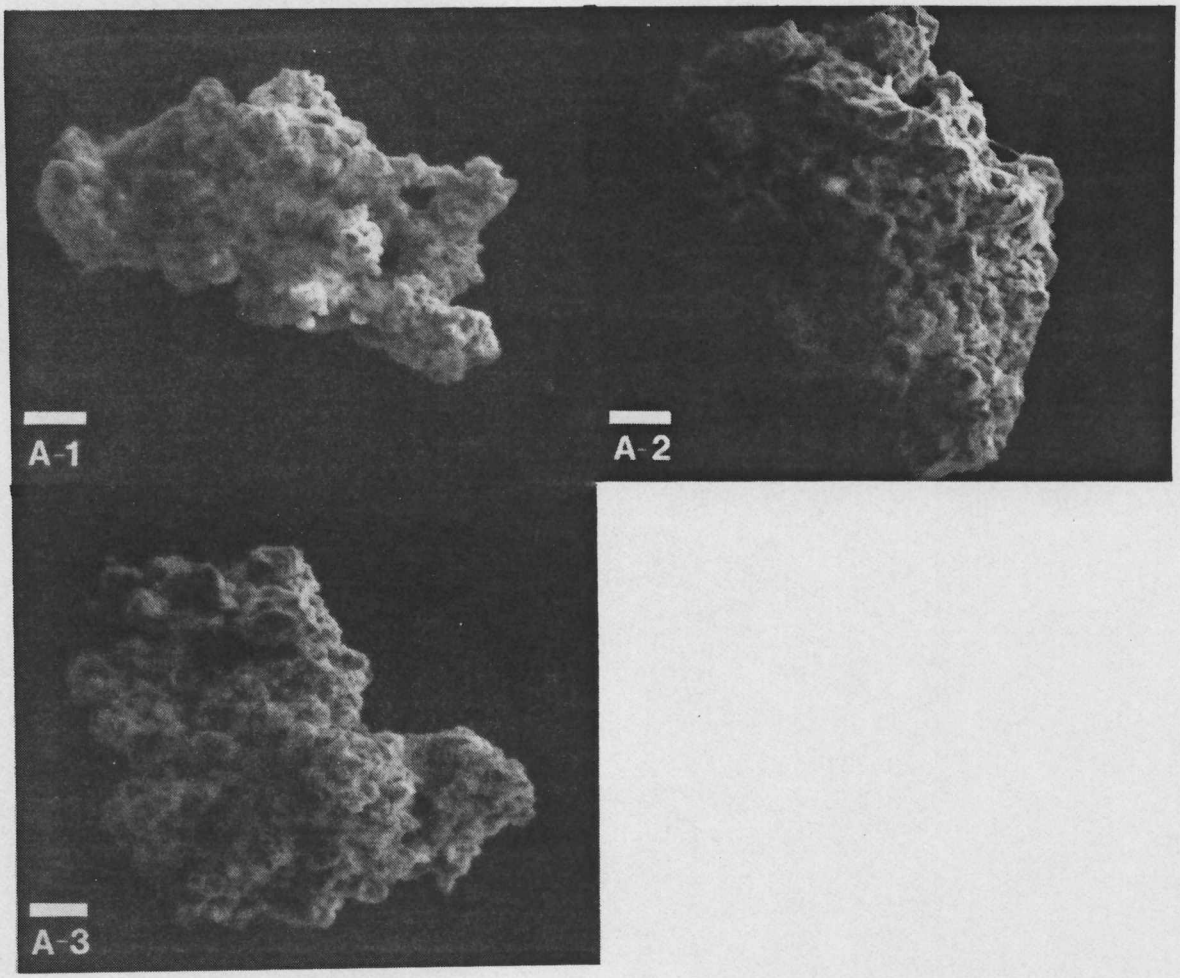
APPENDIX A

APPENDIX A

AGGLUTINATE PARTICLES

Agglutinate particles consist of small fragments of rock, mineral, meteorite, and glass bonded with a glass produced during micrometeorite impacts. Their abundance in a soil reflects the relative exposure age of that soil (i.e. the higher the abundance, the longer the exposure).

See A-1 (14163,76-25; bar = 50 μm), A-2 (14163,76-26; bar = 50 m), and A-3 (14163,76-27; bar = 50 μm).


A-1
A-2
A-3

APPENDIX B

APPENDIX B

VOLATILE-RICH MICROMOUND COATINGS ON VOLCANIC BEADS

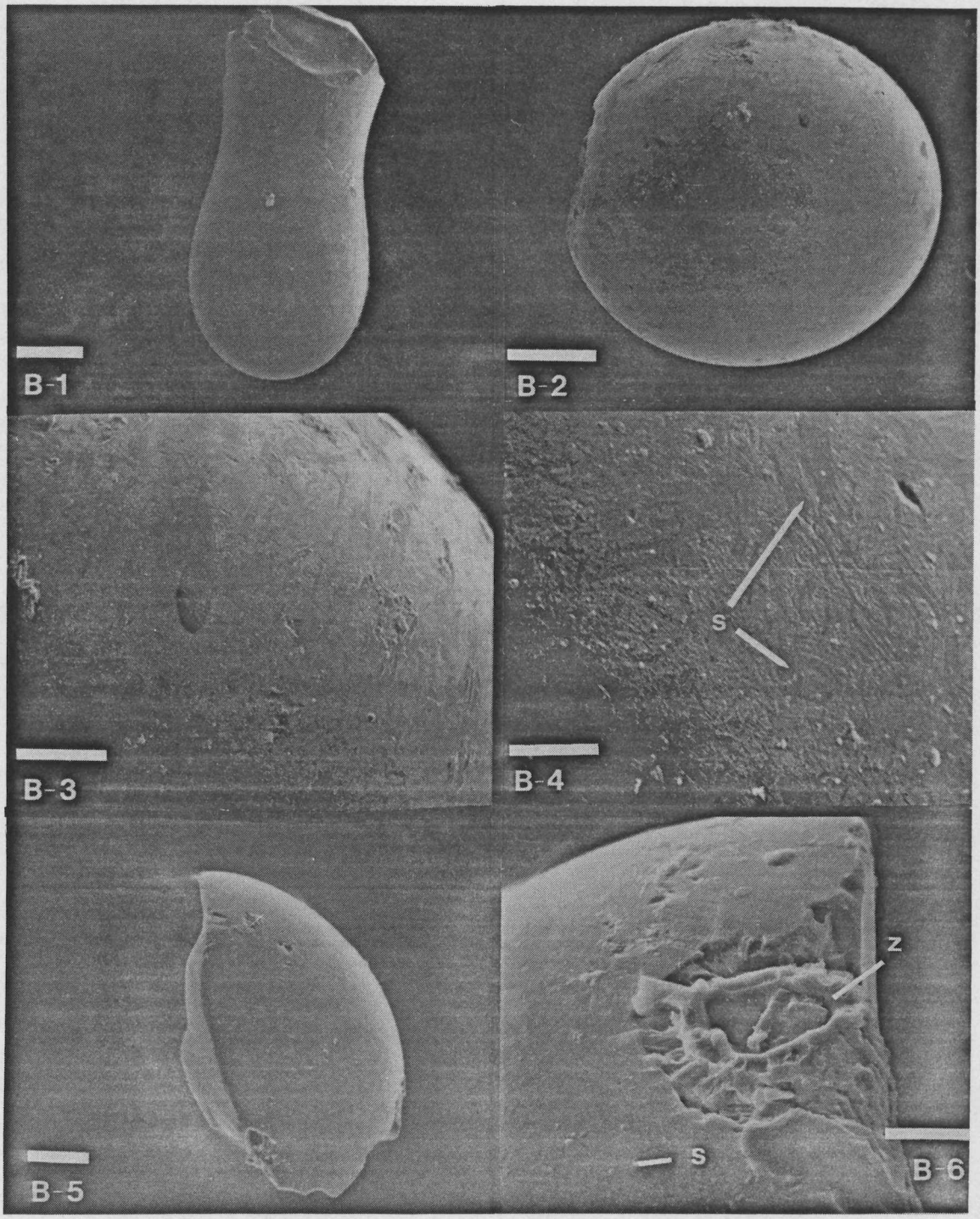
Energy dispersive X-ray analyses indicate the presence of S, Zn, Cl, and other volatile elements which comprise these micromounds. The coatings are probably remnants of the propulsive gases involved in the fire-fountaining.

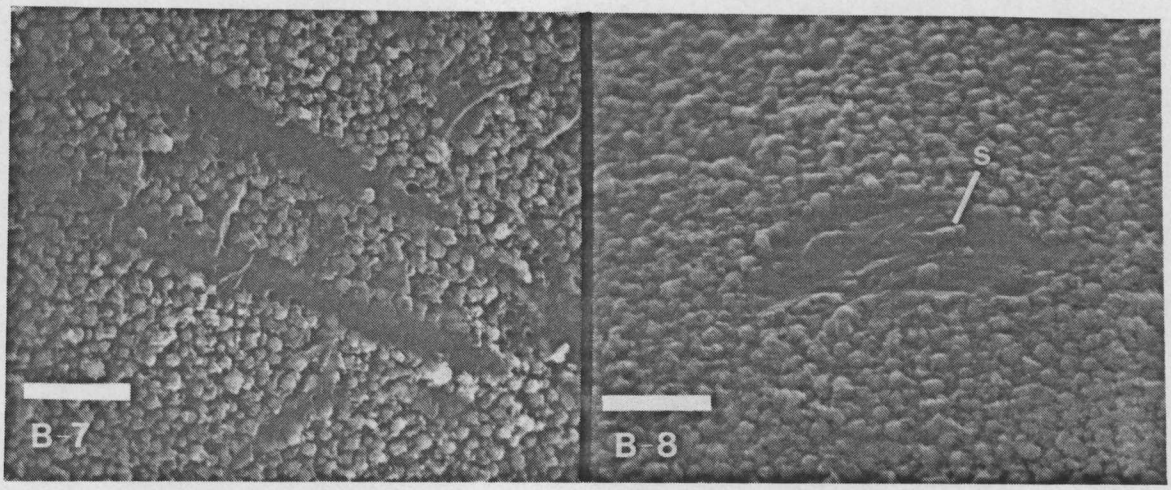
B-1 (74220,6-106; bar = 50 μm) and B-2 (74002,176-128; bar = 50 μm): At low magnification, the micromound coatings appear as mottled surfaces.

B-3 (74002,176-128; bar = 20 μm) and B-4 (10084,853-142; bar = 5 μm): Higher magnification shows the dark areas to be abrasions and scrapes (s) in the volatile coatings due to mutual collisions during fire-fountaining.

B-5 and B-6, (both 14148,23-38; bars = 50 μm and 20 μm, respectively): A volatile-rich surface coating reveals this reworked fragment to be volcanic. A zap pit (z) in B-6 shows an impact-glass lined crater probably responsible for the fragments's elevated I_s value. Note volatile micromound texture and scrapes (s) in lower left of B-6.

B-7 and B-8 (both 64002,262-162; bars = 2 μm and 1.5 μm respectively): A very unusual and rare volatile micromound deposit. Its thickness is unprecidented in the volcanic beads previously analyzed. Abrasion indicates that the mounds were plastic as they were scraped and smeared over the glassy substrate (s) in B-8.


B-1
B-2
B-3
S
B-4
Z
S
B-5
B-6


B-7
B-8
S

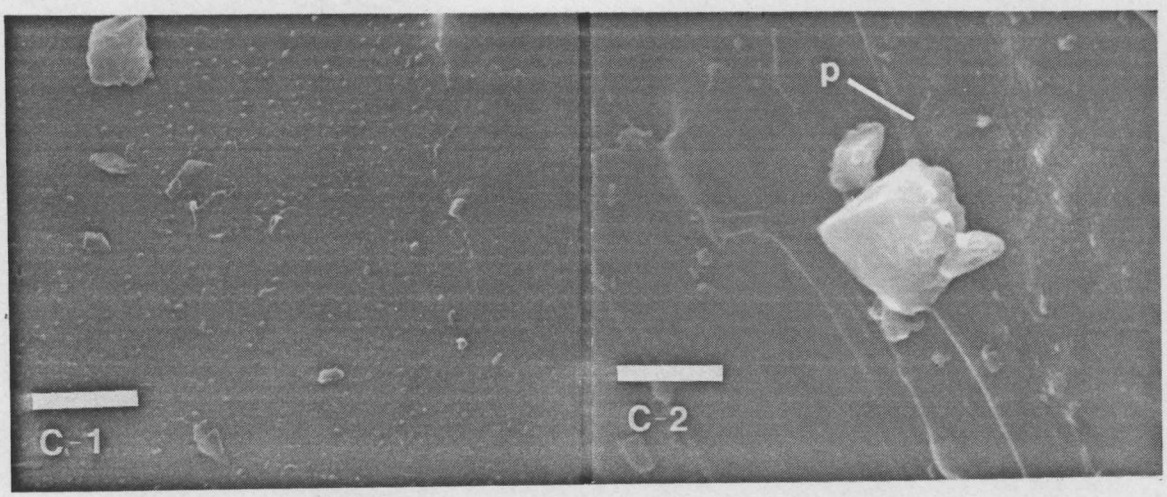
APPENDIX C

APPENDIX C

Fe-RICH PLATELETS ON VOLCANIC BEADS

Small, Fe-rich (80-90 wt%) particles are imbedded in the grain surfaces of some volcanic beads. These are primary features as many are coated with volatile micromounds indicating penecontemporaneous formation at time of fire-fountaining.

C-1 and C-2 (both 15401,14-75; bars = 2 μm): Platelets are visible as small, light-colored mounds on much of C-1 and on the right side of C-2 (p).



APPENDIX D

APPENDIX D

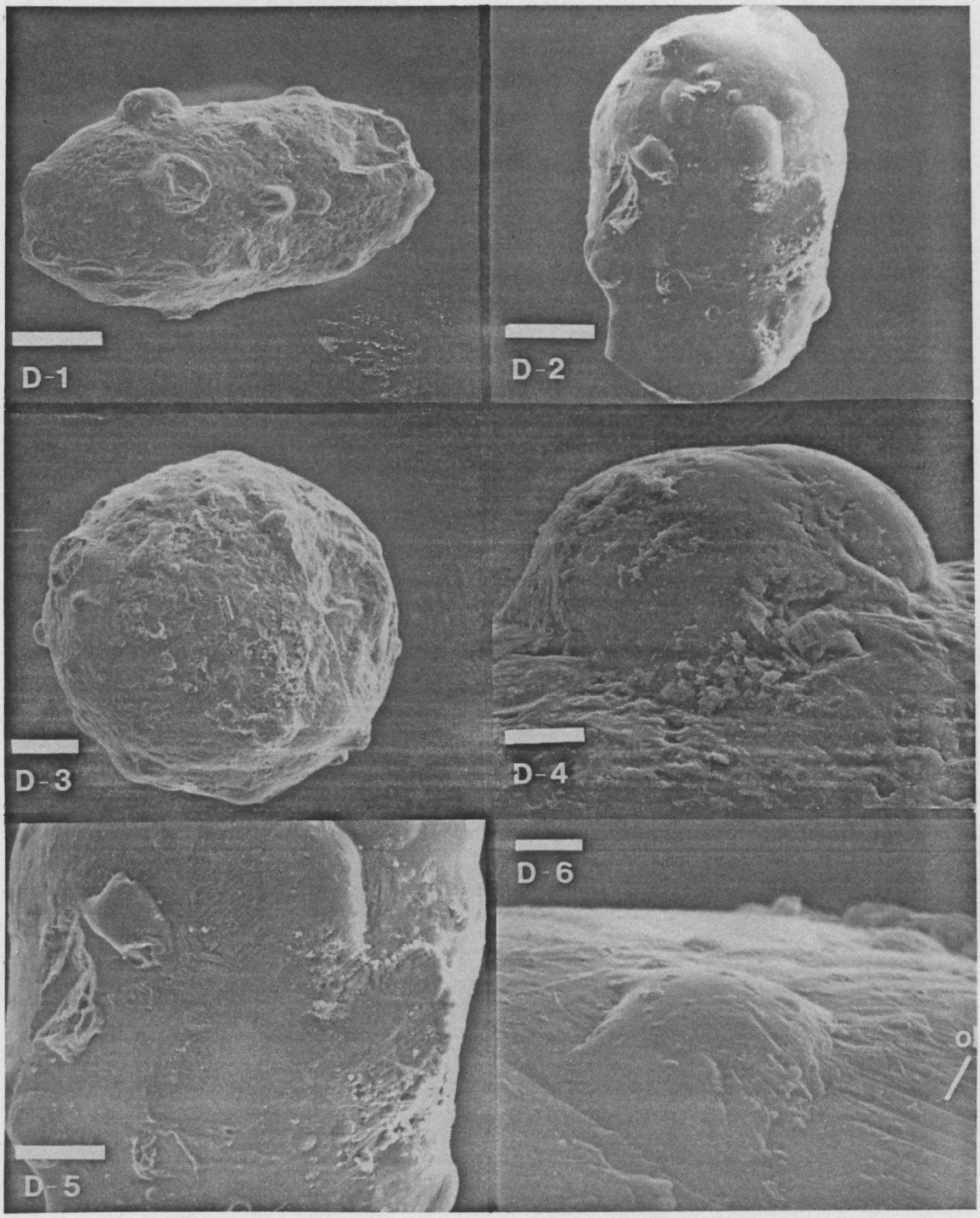
VOLCANIC COMPOSITE MORPHOLOGY

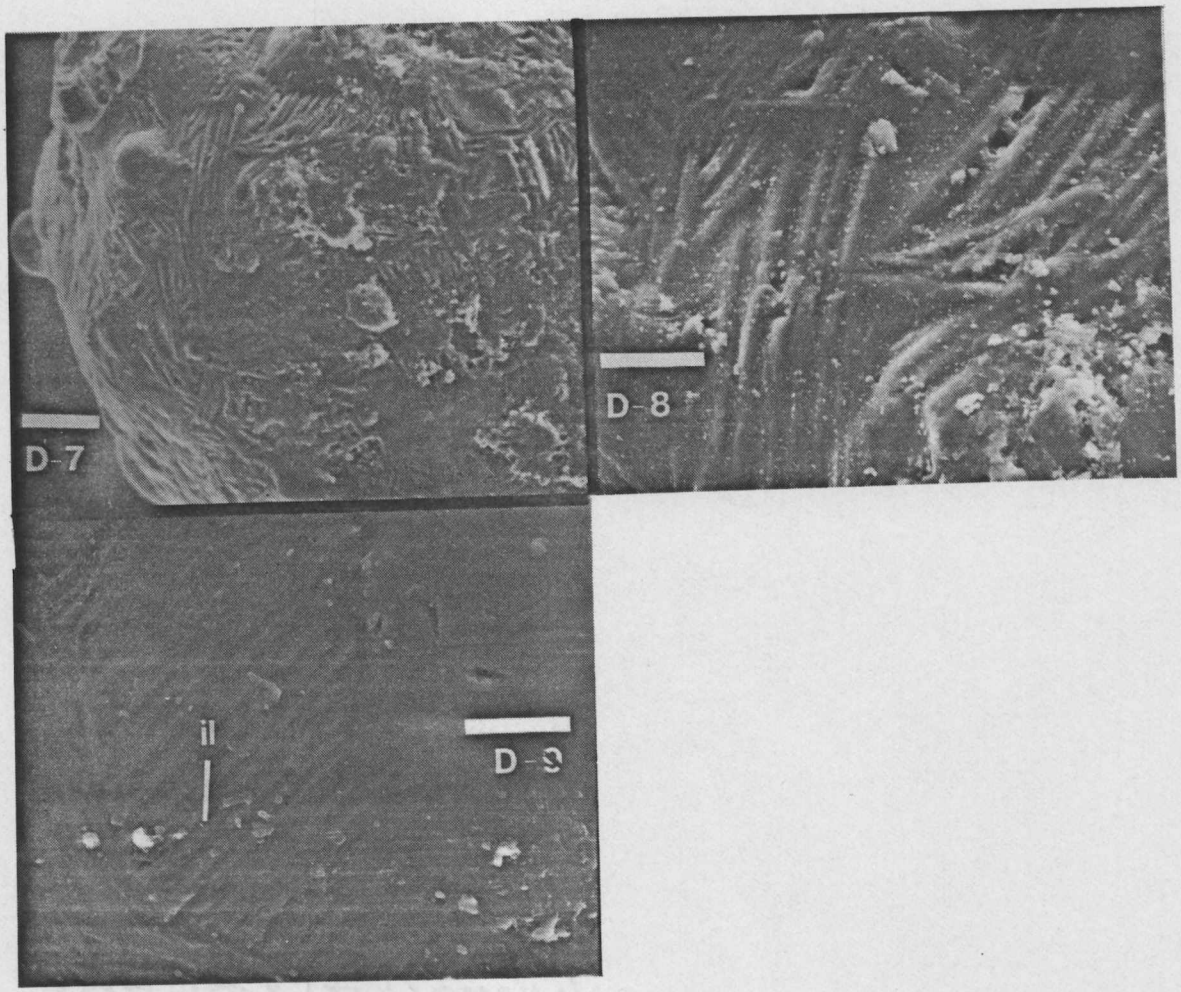
Composite morphology is due to processes which occurred during an early phase of fire-fountaining. Globules of magma collide and adhere to each other or to larger host grains, forming larger, irregular grains.

D-1 (74001,2-12; bar = 200 μm), D-2 (74220,6-18; bar = 100 μm), and D-3 (74001,2-11; bar = 25 μm): Though the particles are generally elongate, spherical grains can also form.

D-4 (74001,2-12; Bar = 40 μm), D-5 (74220,6-18; Bar = 20 μm), and D-6 (74220,6-19; bar = 5 μm): The degrees of wetting of the globules with the substrate are variable. Factors responsible for this phenomenon are velocity of impacts and viscosity of globules and substrate.

D-6, D-7 (74001,2-11; bar = 50 μm), D-8 (74001,2-11; bar = 20 μm), D-9 (74220,6-18; bar = 20 μm) and D-10 (15401,14-75; bar = 10 μm): Devitrification of the composite grains is common. They are maintained at high temperatures long enough to allow precipitation of feathery ilmenites (il) and barred olivines (ol).


D-1
D-2
D-3
D-4
D-5
D-6


D-7
D-8
il

APPENDIX E

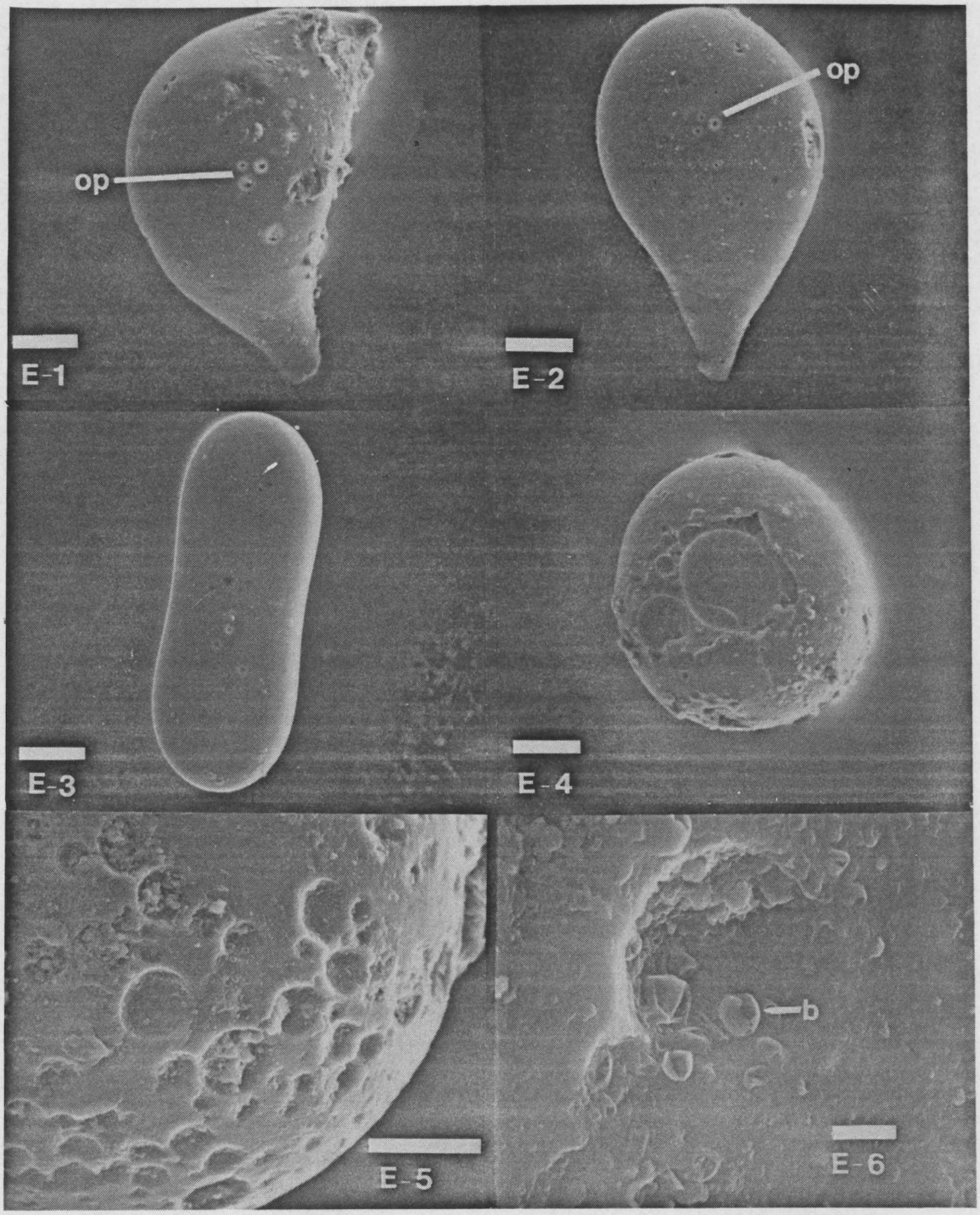
APPENDIX E

OUTGASSING PORES ON IMPACT GLASSES

Glass beads of impact origin generally are vesicular. The vesicular features are actually outgassing pores produced by the escape of volatile gasses generated during an impact.

E-1 (10084,853-79; bar = 50 μm), E-2 (10084,853-87; bar = 50 μm), E-3 (10084,853,-92; bar = 50 μm), and E-4 (14148,23-25; bar = 50 μm): The size of the outgassing pores (op) and the shape of the bead vary widely for the impact droplets.

E-5 (14003,28-63; bar = 20 μm) and E-6 (14003,28-63; bar = 2 μm): This sample has a large population of pores. A close-up of one area (E-6) reveals the formation of minute, thin-walled bubbles (b), many of which burst while still hot, as is evident from the plastic fashion in which the walls of the bubbles collapsed.


op
E-1
op
E-2
E-3
E-4
E-5
b
E-6

APPENDIX F

APPENDIX F

AUTO-REDUCED NATIVE Fe MICROMOUNDS ON IMPACT BEADS

Fe micromounds exist as surface features on beads of impact origin. They are the direct result of auto-reduction of Fe^{2+} in a silicate melt produced through meteoritic impacts.

F-1 (14148,23-34; bar = 20 μm), F-2 (64002,263-119; bar = 4 μm), and F-3 (64002,264-121; bar = 2 μm): The white, rounded mounds are the Fe features (Fe). The size of the micromounds can vary greatly on the same bead. Many exceed the limit of resolution of measurement (generally <200Å).

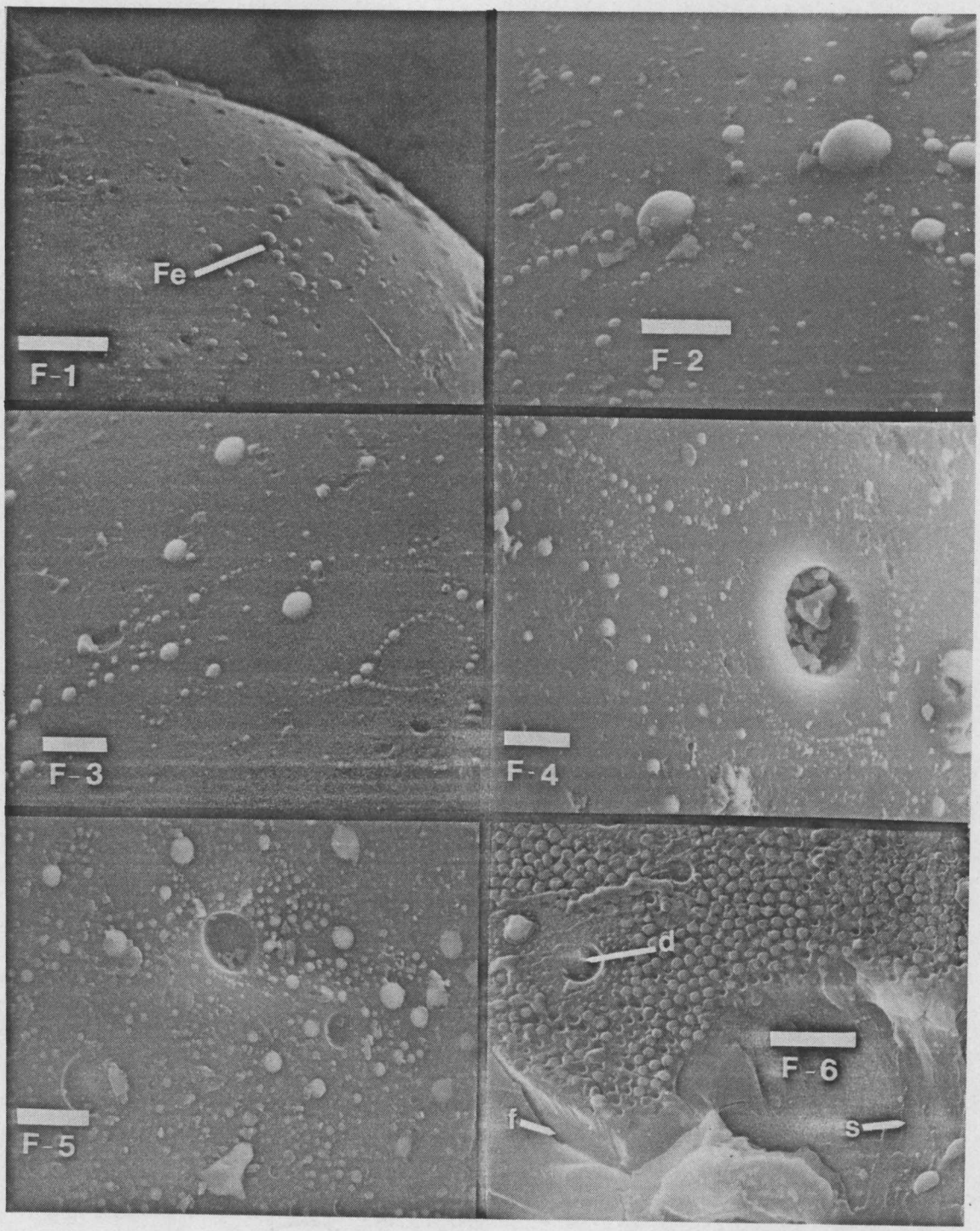
F-4 (14156,23-168; bar = 5 μm) and F-5 (64002,266-158; bar = 5 μm): The mounds frequently occupy areas around outgassing pores which further suggests the mechanism of auto-reduction involves the gases evolved during the melt phase.

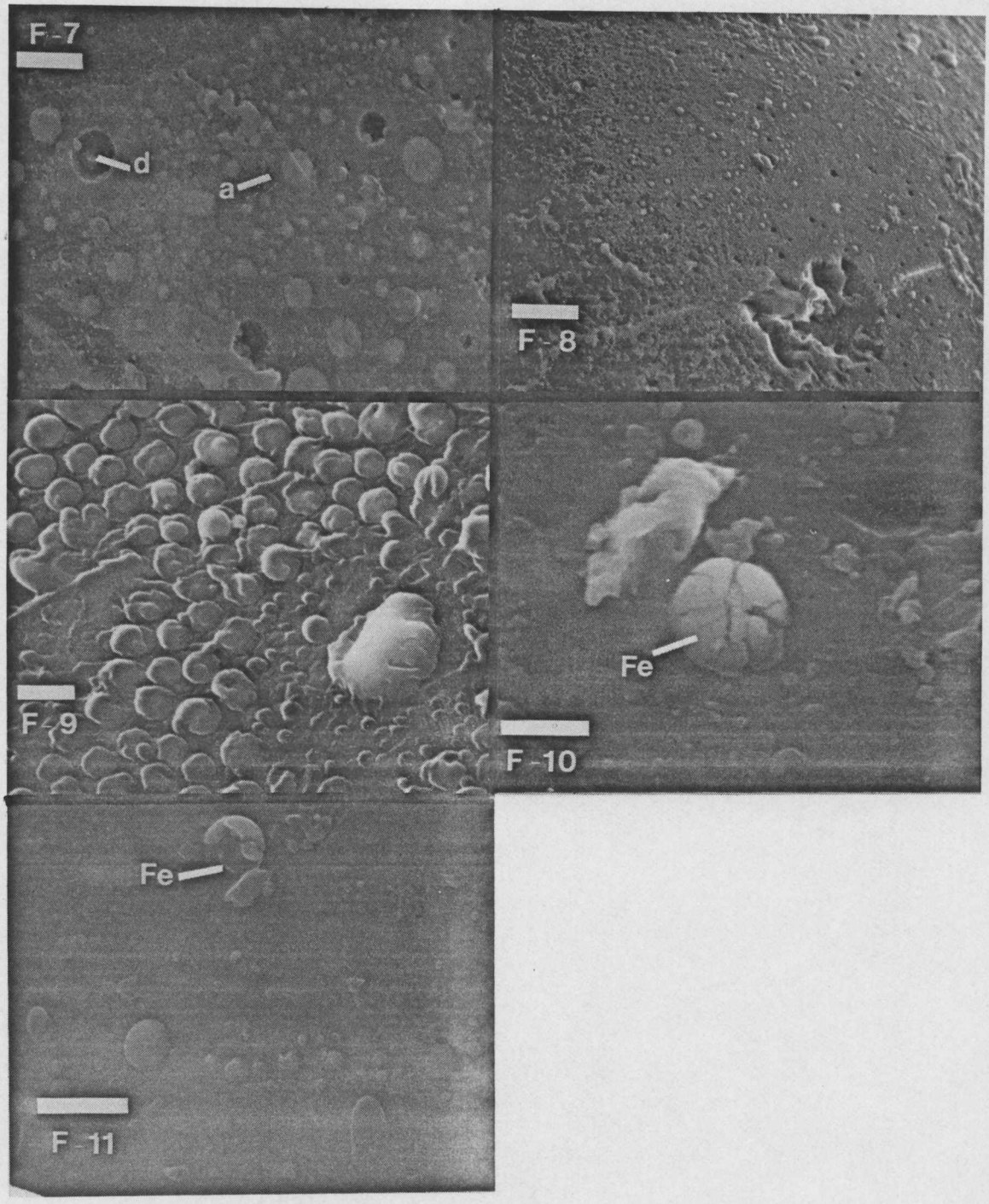
F-6(10084,853-4; bar = 5 μm) and F-7 (10084,853-86; bar = 5 μm): Other depressions (d) among the micromounds represent cavities left after some of the larger Fe mounds were plucked from the surface. Perhaps, this is due to shock imposed on the bead by processes involved in reworking. F-6 shows evidence of reworking in the fractures (f) and sintering (s) of glass at the bottom. F-7 also has been reworked. Shearing of mounds at the surface caused some plucking; also note secondary glass accretion (a).

F-8 (10084,853-4; bar = 20 μm) and F-9 (10084,853-4; bar = 1 μm):

This distribution of Fe micromounds exhibits a pattern similar to those formed by condensation. Evenly distributed mounds are interupted by larger mounds which are surrounded by much smaller ones.

F-10 (10084,853-82; bar = 2 μm) and F-11 (64002,262-117; bar = 2 μm): Some of the Fe micromounds appear to have experienced shock damage as evidenced by fractures (Fe). F-11 has a micromound which has been broken apart and reveals an internal cavity (Fe). This suggests that some Fe micromounds may be hollow.


Fe
F-1
F-2
F-3
F-4
F-5
d
F-6
f
s


F-7
d
a
F-8
F-9
Fe
F-10
Fe
F-11

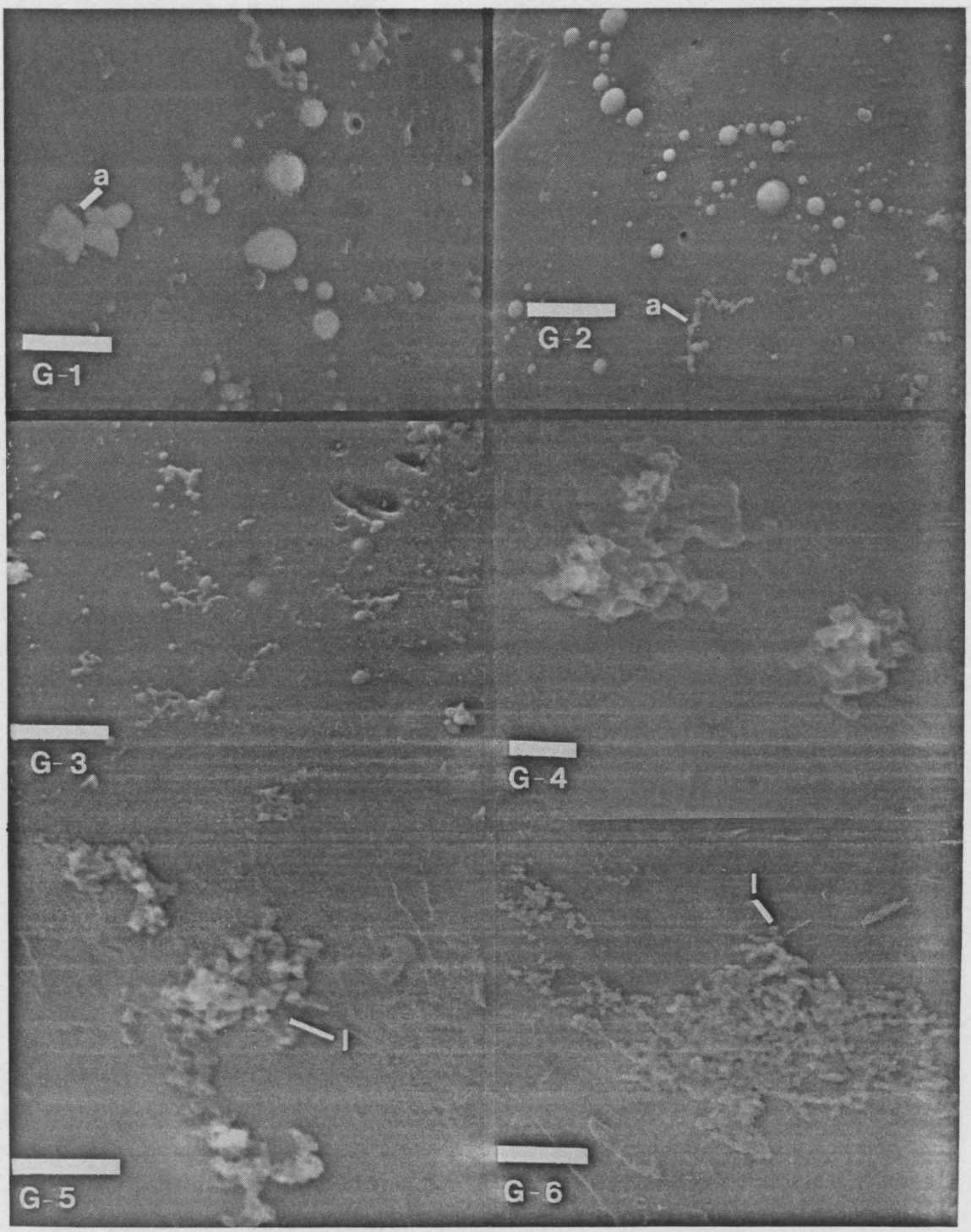
APPENDIX G

APPENDIX G

FORMATIONS OF AMOEBOID/"LACY" IRON ON IMPACT BEADS

Amoeboid and "lacy" iron formations comprise the end members of a spectrum of native-Fe morphologies formed from direct condensation from from a vapor related to impacting.

G-1 (10084,853-87; bar = 10 μm), G-2 (12070,104-156; bar = 5 μm), G-3 (12070,29-50; bar = 4 μm), G-4 (10084,853-79; bar = 5 μm), G-5 (10084,853-8; bar 1 μm), G-6 (10084,853-8; bar = 1 μm), and G-7 (10084,853-8; bar = 2 μm): The spectrum at one end, can be represented by G-1. A blocky ameoboid morphology (a) is dominant with some psuedo-hexagonal shapes apparent. A continuity extends through the spectrum to G-7 where iron has formed a delicate, "lacy", three-dimensional network (1).

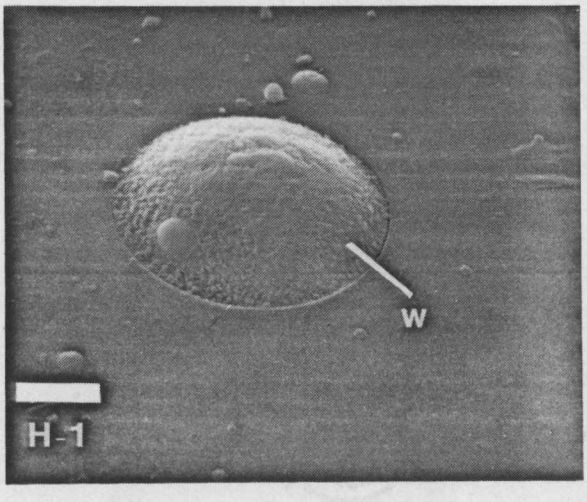

a
G-1
a
G-2
G-3
G-4
l
G-5
l
G-6

APPENDIX H

APPENDIX H

IRON MICROMOUNDS WITH VOLATILE "WAISTS" ON IMPACT BEADS

These features are formed by the same processes as the other Fe micromounds. However, an added aspect is the textured volatile coating which generally is confined to near the mound/bead interface as seen in H-1 (10084,853-150; bar = 2 μm). The volatile "waists" (w) are rich in S and P.



APPENDIX I

APPENDIX I

SECONDARY IMPACTS ON GLASS BEADS

Secondary impacts occur after the initial formation of a glass bead. The amount of time after formation may be very short or occur after AE's (reworking). The morphology of the impact site differs according to the viscosity differences between the target and the projectile and the relative velocities.

I-1 (15401,14-145; bar = 10 μm) and I-2 (15401,14-71; bar = 2 μm): These "finger-print" splashes are on volcanic beads. The projectiles were molten glass which impacted an already solidified bead.

I-3 (15401,14-146; bar = 20 μm): This impact also occurred on a volcanic bead. It has undergone deformation which was partially brittle (d) under the force of impact.

I-4 (15401,14-14; bar = 5 μm) and I-5 (14148,23-17; bar = 10 μm): Sometimes the glass projectile may be semi-soft and survive the impact more completely. The remnants of the projectiles are often seen (r).

I-6 (10084,853-136; bar = 10 μm) and I-7 (10084,853-81; bar = 2 μm): Impacts of relatively low velocities between semi-soft projectiles or targets often leave craters. I-6 shows an impact by a semi-soft projectile. The remnants of the projectile are visible around the crater. I-7 shows a central crater with ejecta rays extending radially

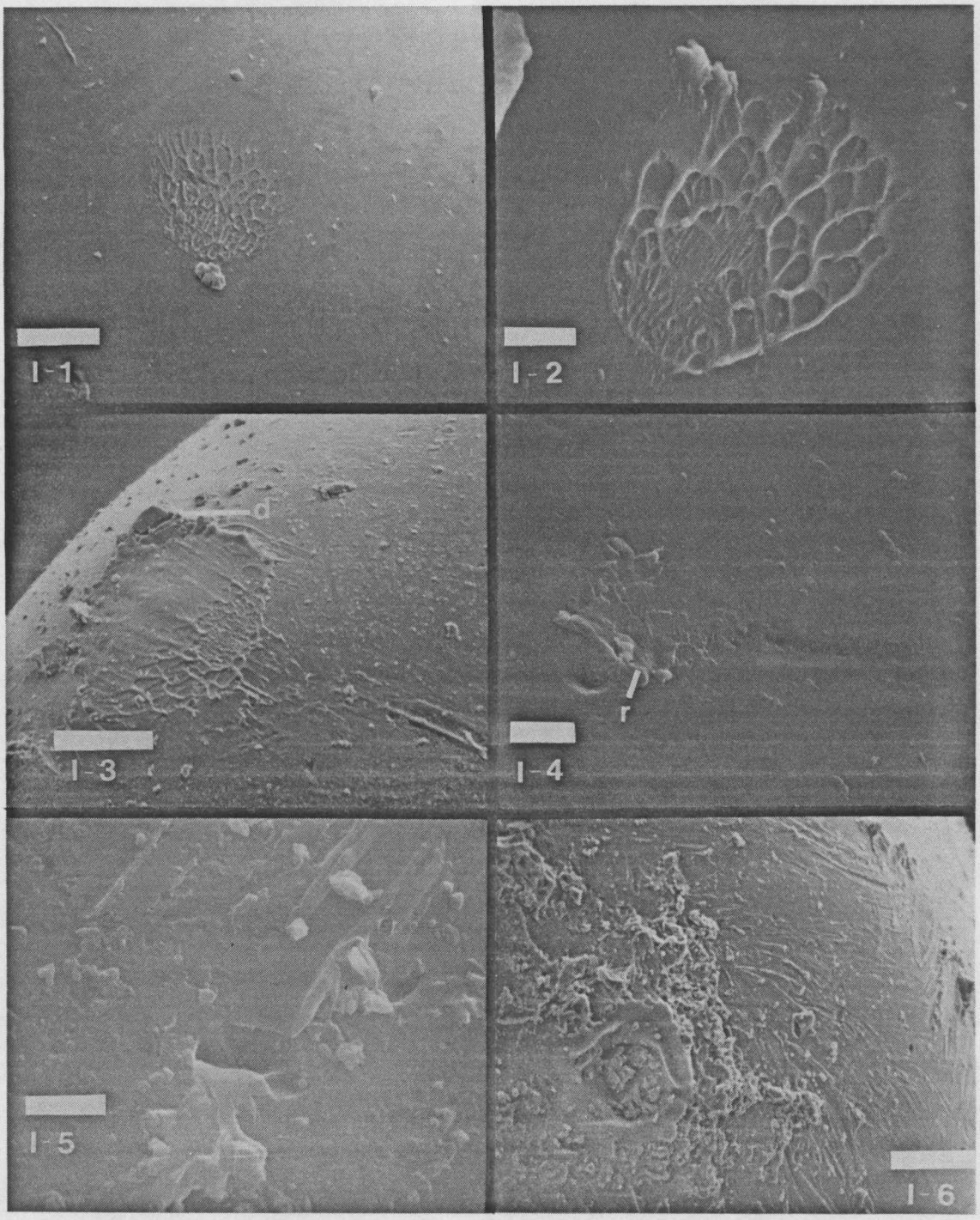
outward from the center (e).

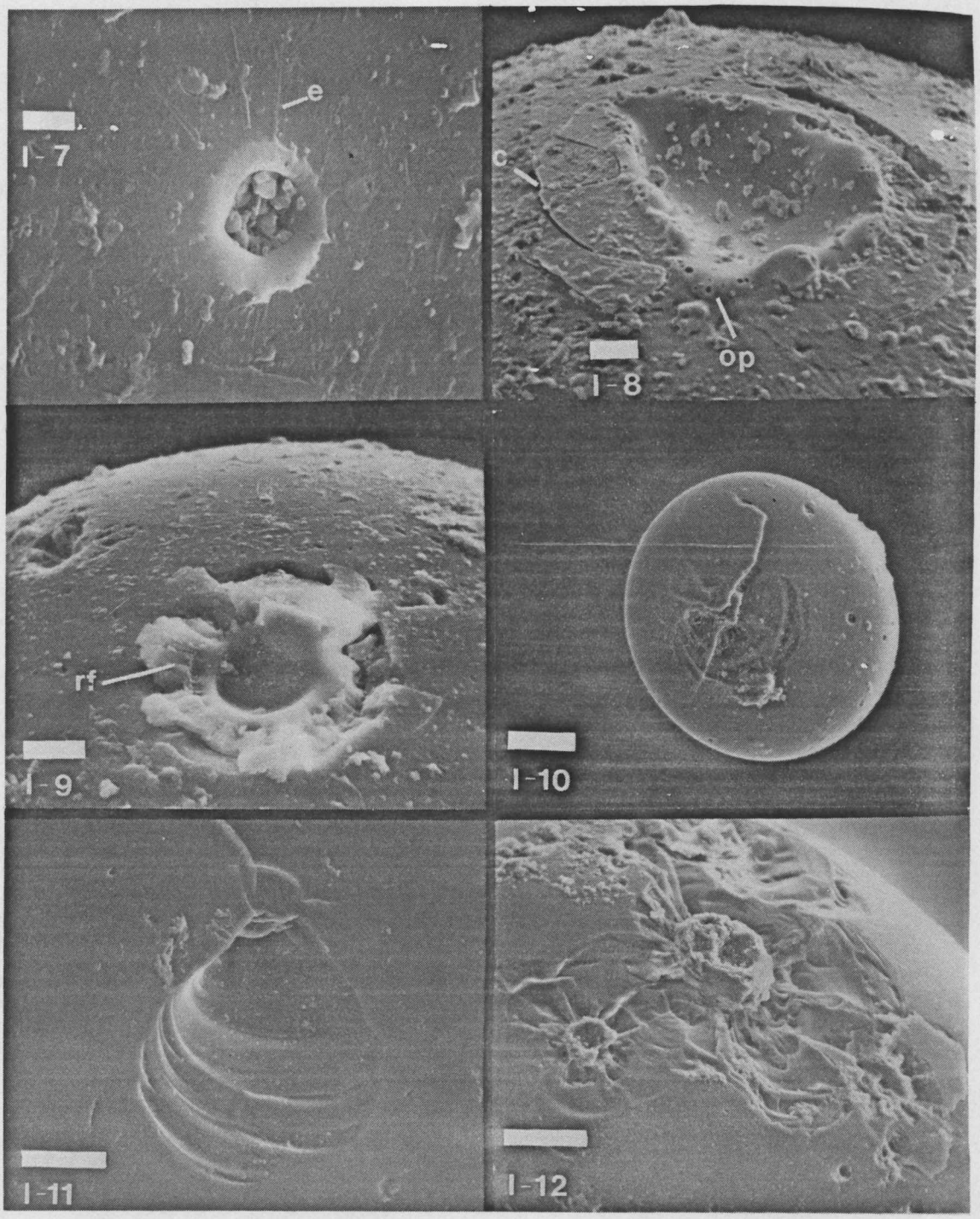
I-8 (10084,853-143; bar = 5 μm): This feature represents a transition stage between low velocity, semi-soft impacts and higher velocity impacts between solid objects which tend to form spalls. Note the partial concentric separation (e) around the impact area. Also, outgassing pores (op) are visible in the impact, glass-lined crater.

I-9 (14148,23-37; bar = 5 μm): Zap pits formed by hyper-velocity impacts generally create concentric separations and radial fractures (rf), as well as a central, glass-lined crater.

I-10 (14156,23-168; bar = 50 μm) and I-11 (15401,14-14; bar = 30 μm): Some hyper-velocity impacts occurring at oblique angles can spall off chips of glass concoidially.

I-12 (14148,23-36; bar = 40 μm): In particularly energetic impacts, melt-glass lined pits, concentric and radial fractures, and spalling can occur at the same time.


I-1
I-2
d
I-3
r
I-4
I-5
I-6


e
I-7
c
op
I-8
rf
I-9
I-10
I-11
I-12

APPENDIX J

APPENDIX J

SURFACE ACCRETIA

Accretia constitute the deposit of glass, regolith, or other foreign material on the surface of the bead.

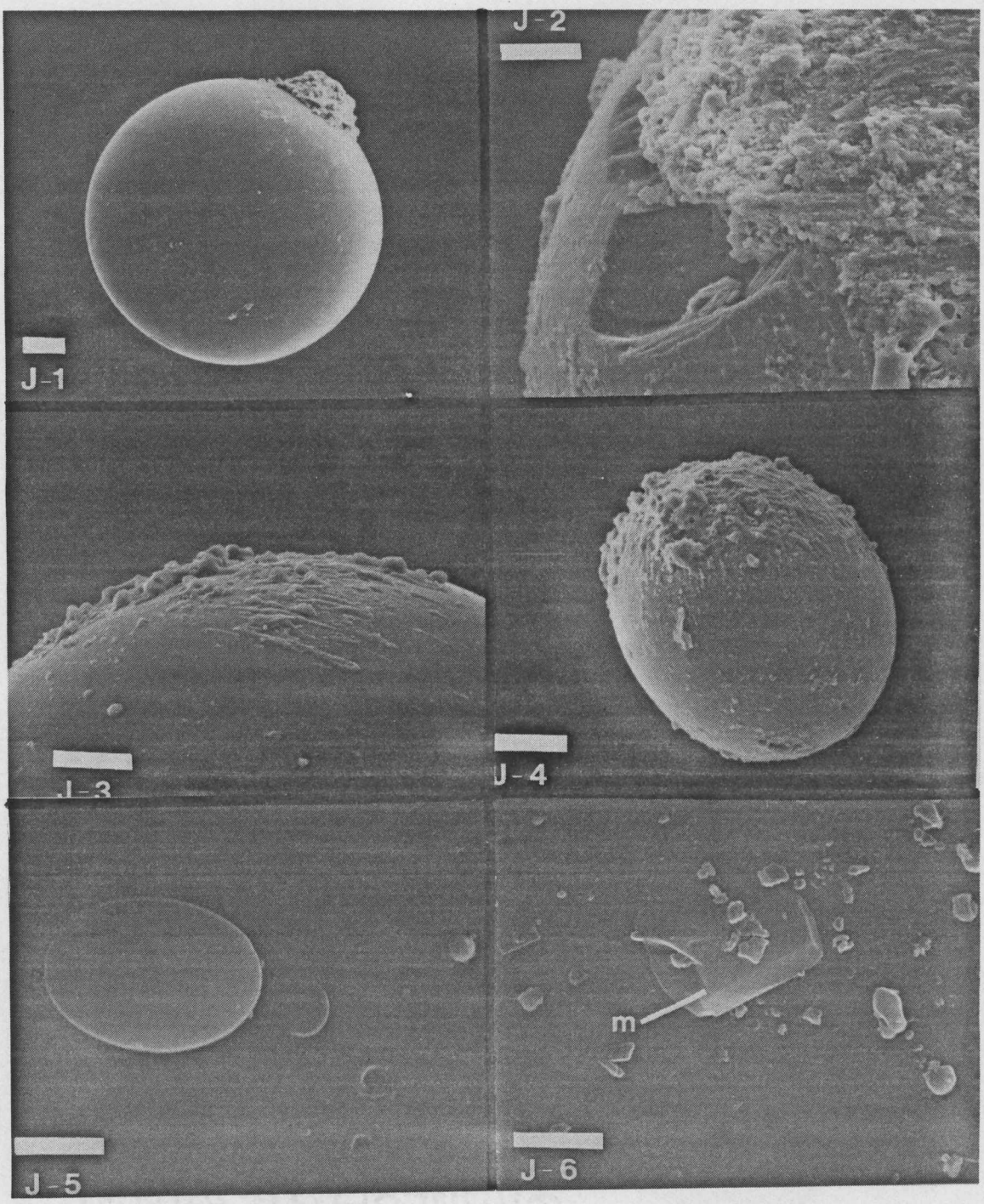
J-1 (18001,7-23; bar = 50 μm) and J-2 (10084,853-8; bar = 30 μm): A glass bead mobilized during large impacts can move through ejecta clouds at high speeds accumulating material on its surface.

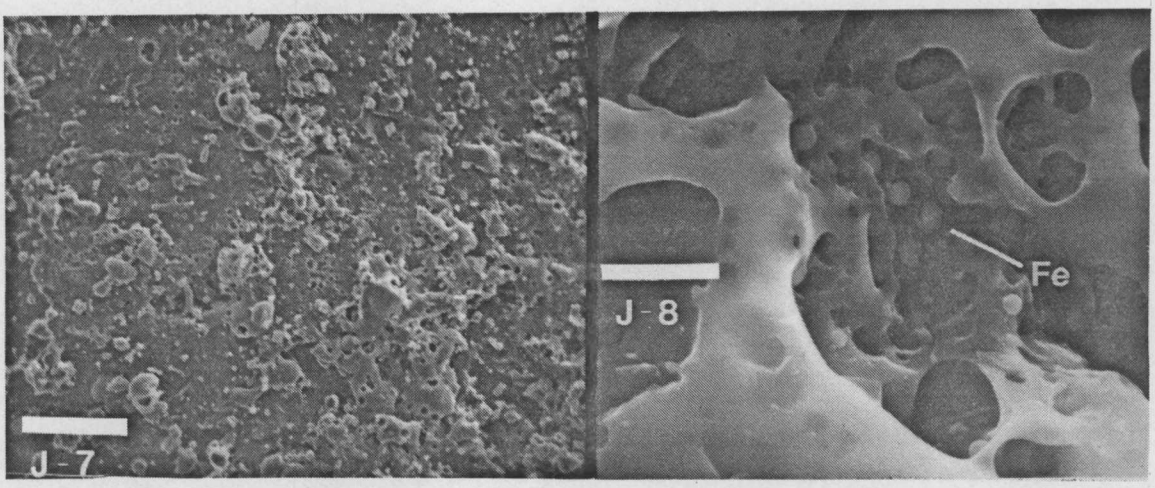
J-3(12070,104-1; bar = 30 μm) and J-4 (10084,853-82; bar = 50 μm): The relative direction of transport of the accretia can often be readily established by cursory inspection. In both of these samples the accretia impacted from the upper left of the photo.

J-5 (12070,104-53; bar = 2 μm): Glass accretia typically form as discs on a surface. Elongate discs indicate an oblique impact.

J-6 (14141,31-165; bar = 2 μm): Mineral grains (m) can also adhere to glass bead surfaces.

J-7 (10084,853-135; bar = 10 μm) and J-8 (10084,853-4; bar = 4 μm): Secondary coatings of surface glass can cover much of a bead. Note the vesicular nature of the coating in J-7. J-8 shows a secondary vesicular coat of glass with the primary surface of Fe micromounds visible below the vesicules (Fe).


J-1
J-2
J-3
J-4
m
J-5
J-6


J-7
J-8
Fe

APPENDIX K

APPENDIX K

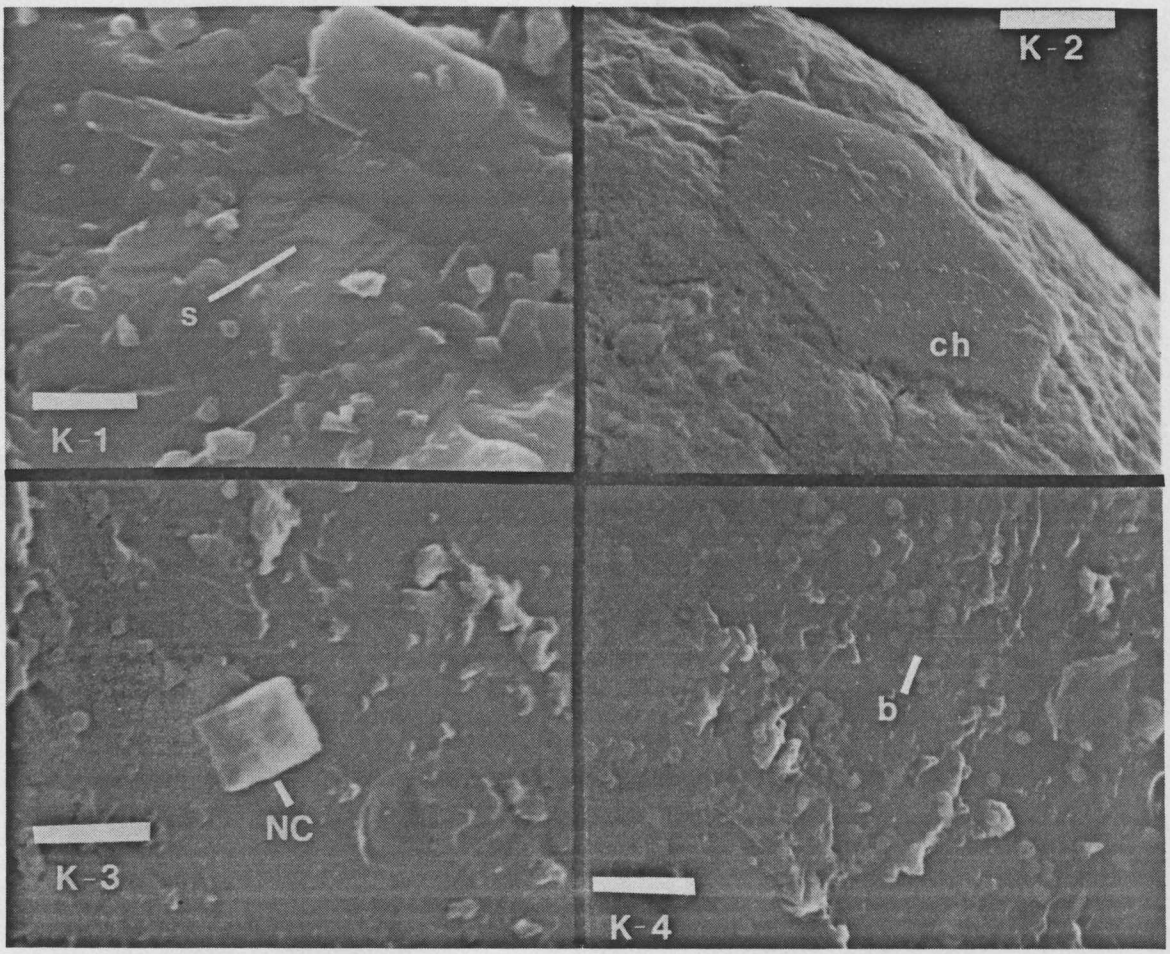
MISCELLANEOUS FEATURES

K-1 (14156,23-59; bar = 1.5 μm): Surface of this bead is covered with crystalline growths. The stair-step nature of the crystals (s) indicates formation by vapor precipitation.

K-2 (64002,261-124; bar = 4 μm): Hexagonal chromite crystal (ch) imbedded in surface of grain.

K-3 (141438,23-39; bar = 2 μm): Crystal of NaCl (NC) on surface of bead, possibly due to terrestrial contamination.

K-4 (14148,23-37; bar = 2 μm): Unidentified bacteria (b) contamination on surface in the form of small spheres. This contamination also probably is terrestrial.


K-1
s
K-2
ch
K-3
NC
K-4
b

VITA

Charles David Stone was born in Brussels, Belgium on January 30, 1955. He attended elementary schools in New York and New Jersey and was graduated from R.E. Lee High School, San Antonio, Texas in May, 1972. He entered Texas A & I University in August 1974. In August 1976 he transferred to the University of Texas at Austin where he received a Bachelor of Science degree in the Geological Sciences in May, 1980. In August, 1980, he entered the Graduate School of the University of Tennessee. He received his Master's of Science Degree with a major in Geology in December 1982.